DESIGN, ANALYSIS, FABRICATION AND TEST OF AN UHF (ULTRA HIGH FREQUENCY) PASSIVE RFID (RADIO FREQUENCY IDENTIFICATION) TAG ANTENNA

BY

SIMRAN SINGH

THESIS

Submitted in partial fulfillment of the requirements
for the degree of Bachelor of Science in Electrical and Computer Engineering
in the Undergraduate College of the
University of Illinois at Urbana-Champaign, 2013

Urbana, Illinois

Adviser:

Professor Jennifer T. Bernhard

ABSTRACT

Obtaining optimal antenna performance can be a great challenge, especially when working with electrically small antennas. This thesis provides an overview of the design, simulation, fabrication and test measurement setup for an ultra high frequency, electrically small, passive, RFID tag antenna operating in the 915 MHz ISM band (902-928 MHz). Key project topics include:

Design motivation in coming up with antenna design.
Design simulations using Ansys HFSS (high frequency structure simulator), which is a commercial, finite element method solver for electromagnetic structures.
Design tradeoffs and constraints.
Fabricating the antenna and taking radiation pattern measurements inside an anechoic chamber using a balun.
Investigating the discrepancies between simulated and measured results and approaches taken to minimize those discrepancies.

At 915 MHz, the fabricated antenna achieves a return loss of 7.39 dB at a bandwidth of 40 MHz, VSWR of 2.4 and an input impedance of $28 + j27\,\Omega$.

Keywords: Tag antenna, RFID, Anechoic Chamber, Return loss, Impedance matching, HFSS, Radiation pattern, Balun, Gain, Aperture size.

To my parents and all the amazing professors at UIUC

ACKNOWLEDGMENTS

Firstly, I am grateful to Prof. Jennifer T. Bernhard for her constant support and guidance not only for this thesis, but also for helping me make some of the important decisions during my time here at University of Illinois. I am extremely lucky to be doing my senior thesis under her guidance.

Secondly, I would like to thank all the Professors at UIUC, specially Prof. Erhan Kudeki. He has always motivated me and guided me in the right direction.

I would also like to thank all the graduate students in the antenna group at University of Illinois especially John, Matt, Aaron and Robert for helping me out, even at strange hours.

TABLE OF CONTENTS

LIST OF TABLES

LIST OF FIGURES

CHAPTER 1

INTRODUCTION

1.1 RFID

RFID stands for radio frequency identification, which is the use of radio waves to communicate and identify a physical object. RFID uses electromagnetic fields to transfer data, for the purpose of automatically identifying and tracking tags attached to physical objects. There are several ways of identification, but the most common is to store a serial number that identifies an object or other information on a chip that is attached to an antenna [5]. (The chip and the antenna are commonly called an RFID tag or an RFID transponder.)

1.2 RFID Components

A typical RFID system consists of a tag and a reader as shown in Figure 1.1. A computer or a host is connected to a reader system, which usually consists of a transmitter and a reader antenna. The reader antenna transmits radio waves to the tag antenna. The tag antenna is tuned to receive these waves. A passive RFID tag draws power from the fields created by the reader and uses it to power the microchip's circuits as explained in [6]. The chip then modulates the waves using load modulation and sends them back to the reader.The reader then converts these radio waves into digital data for post processing and identification.

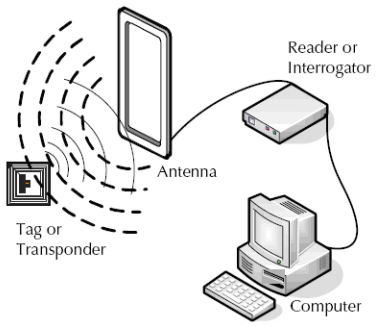

Figure 1.1: A typical RFID system [1]

1.3 Types of RFID Systems

RFID systems are classified based on the frequency of radio waves they use, by the means of tag power options, or by the protocols used to communicate between the tag and the reader. All the above-mentioned factors have important implications for range, cost and features available to the user. Two common basis of classifying an RFID system are discussed below.

1.3.1 Classification of RFID systems based on frequency bands

RFID systems use frequencies ranging from around 100 kHz to over 5 GHz. Systems rarely operate arbitrarily across this entire range. Most of the systems are concentrated in fairly narrow bands because those bands are unlicensed and free to use based on the decision of regulatory bodies such as FCC. Some common frequency bands used in practice are

- 125-134 kHz
- 13.56 MHz
- 860-960 MHz
- 2.40-2.45 GHz.

The 125-134 kHz systems operate within the low frequency (LF) band. 13.6 MHz systems operate in the high frequency (HF) band. Readers and tags in the 860-960 MHz and 2.4-2.45 region both lie in the UHF(ultra high frequency) region which ends at 3 GHz. The antenna designed in this thesis is for 915 MHz and is thus in the UHF (Ultra High Frequency) band. 915 MHz was chosen as the operating frequency because the ISM band (902-928 MHz) is unlicensed and free to use. Another reason for choosing this frequency was the availability of many commercial RFICs at this frequency.

Corresponding to the range in frequencies, we can also characterize an RFID system based on its operating wavelength. Recall that electromagnetic waves travel in vacuum at the speed of light, c = 299,792,458 m/s. Wavelength (λ) and frequency (f) are related by speed of light (c) through the formula:

$$\lambda = \frac{c}{f} \tag{1.1}$$

From (1.1) it is clear that wavelength is inversely proportional to the frequency. Thus higher the frequency, shorter the wavelength. RFID systems generally have wavelength ranging from as low as 0.03 meters to 3000 meters. Table 1.1 summarizes the frequency band, frequency range and the common frequency used for RFID applications.

Table 1.1: Common RFID frequency band, range and use

Frequency Band	Frequency Range	RFID Frequency Use
Low frequency (LF)	30 kHz to 300 kHz	125 kHz
High frequency (HF)	3 MHz to 30 MHz	13.56 MHz
Ultra high frequency (UHF)	300 MHz to 3 GHz	868 MHz, 915 MHz

Choosing the correct frequency of operation for an RFID system is one of the most important factors relating to the antenna design. At high frequencies the size of the antenna becomes smaller. A trade-off has to be made between the frequency of operation and the read range of the system. If we use a lower frequency, we will have a shorter read range but the antenna design would not be complex. If we use a higher frequency we can get a much larger read range but antenna design would be complex due to small size at higher frequency. The section below highlights the tradeoffs between choosing one frequency band over another.

Tradeoffs between the selection of frequency bands and tag antenna complexity:

- Low frequency (LF) tags use coil antennas with many turns.
- High frequency (HF) antennas need fewer turns. This is because when you increase the number of turns you increase the electrical length of the antenna. That in turn increases the wavelength and consequently decreases the frequency.
- Ultra high frequencies (UHF) tags use simple dipole-like antennas that are

easy to fabricate, but their size tends to be a constraint in their antenna design.

- LF tags are limited to low data rate, whereas as HF and UHF have a higher data rate (usually tens or hundreds of kbps).

Figure 1.2 shows some of the common tag antennas designed for LF, HF and UHF. Low frequency tags use coil antennas with many turns. High frequency tag antennas have fewer turns.

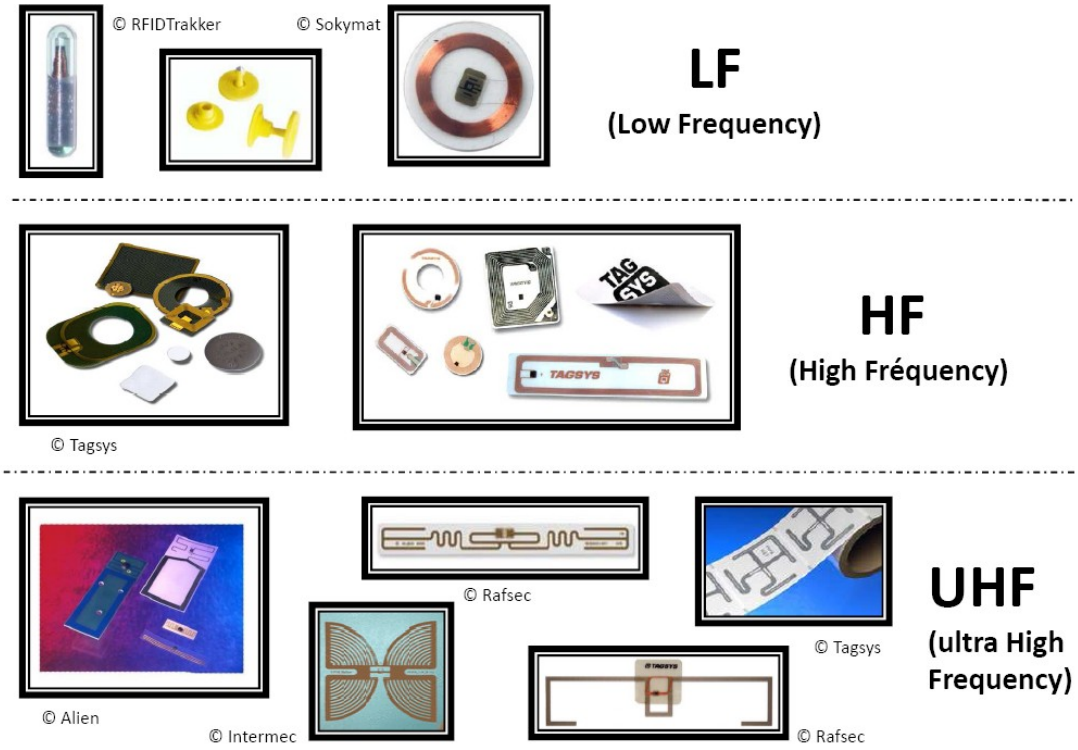

Figure 1.2: Tag antenna designs for LF, HF and UHF systems [2]

Another way to classify RFID systems is based on their options for tag power/transmit configuration. Figure 1.3 describes this classification.

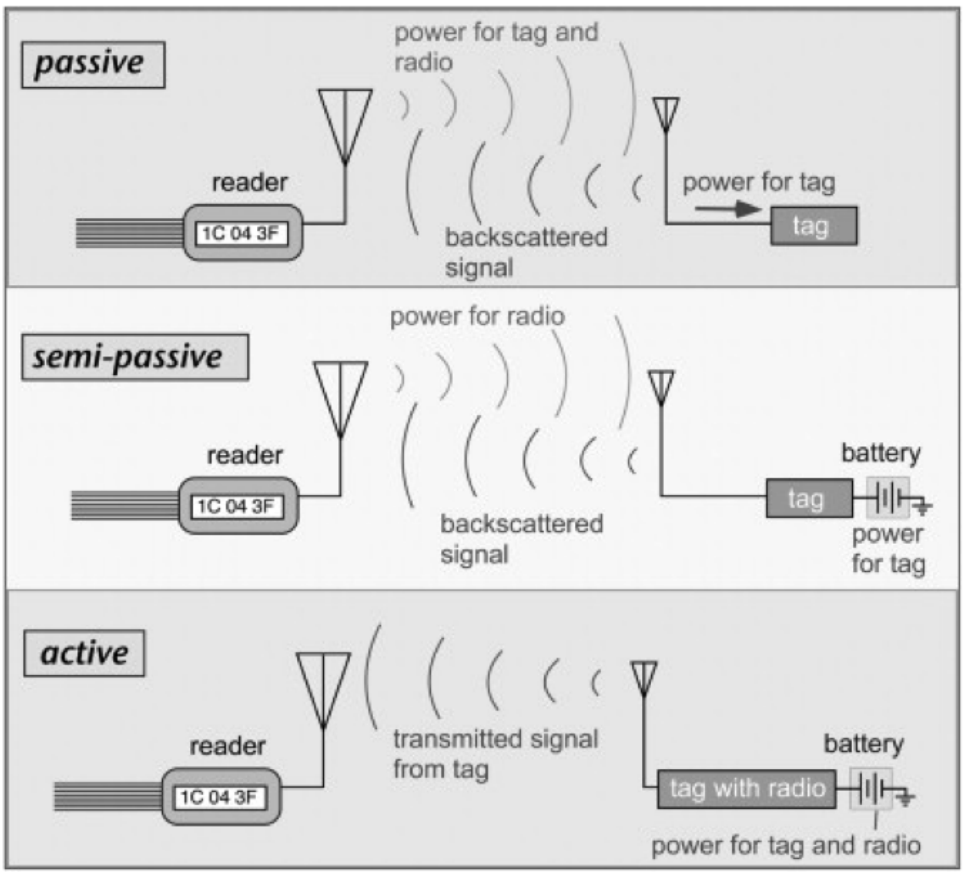

Figure 1.3: Classification of RFID systems based on tag power options [3]

A tag is passive if it does not have its own battery or power source. The tag is powered on by the energy stored in the electromagnetic waves sent by the reader. If the tag has its own battery source but still uses the backscattered signal to send signals to the reader then it is classified as a semi-passive tag. An active tag transmits it's own signal rather than using the backscattered signal.

CHAPTER 2

DESIGN PROCESS

This chapter describes the design process, which includes the motivation behind the design and the steps taken to reach the final design. Design goals, constraints, optimization and comparison of some commercial RFID tag antennas are also discussed in this chapter.

2.1 Design Motivation

Figure 2.1 shows some common types of commercial RFID tag antennas.

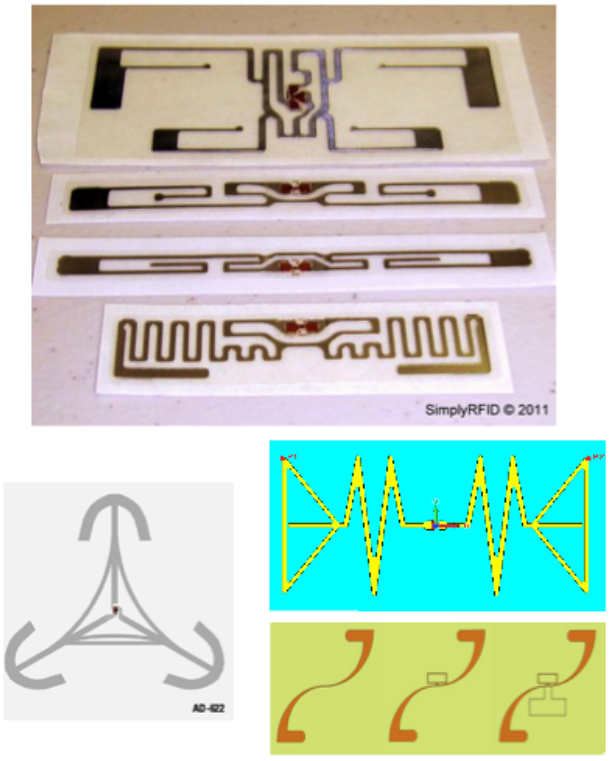

Figure 2.1: Common commercial RFID tag antennas

All the tag designs shown in Figure 2.1 are complex and not intuitive. The design motivation for this thesis was the most basic and fundamental antenna - a dipole. The following section highlights the problem of using a dipole at 915 MHz and the steps taken in going from a dipole to a RFID tag antenna.

At an operating frequency of 915 MHz, a half-wave dipole would be 16.32 cm long. Common RFID tag antennas are used for tracking objects or tracking inventory. For either case, a 16.32 cm long tag would be too large and not optimal. Achieving a good conjugate match to the RFIC chip would also not be possible if we just used a half wave dipole.

As mentioned in chapter 1, common RFID tag dimensions are less than 8 cm x 3 cm. To put a dipole which is 16.32 cm long onto a tag which is 8 cm long, we squeeze the dipole from both sides such that it fits onto an 8 cm long tag. Figure 2.2 and 2.3 describe this in detail:

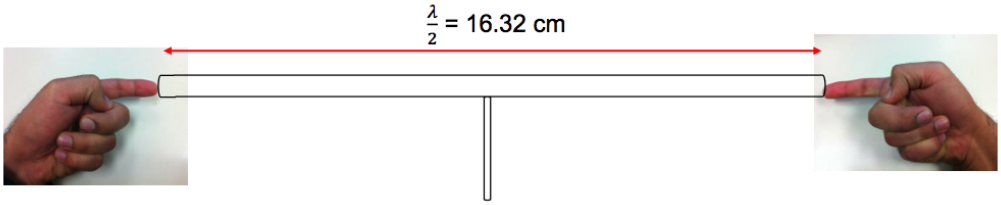

Figure 2.2: Half-wave dipole before squeezing

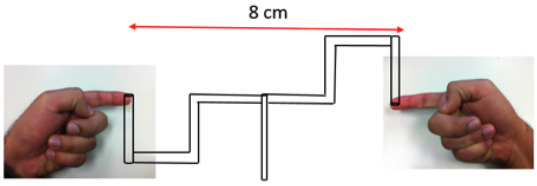

Figure 2.3: Half-wave dipole after squeezing [3]

After squeezing the dipole, an antenna with meandered line structure is obtained. Hence we now get an antenna which is of right size for our application. Figure 2.4 shows both the original 16.32 cm long dipole designed in HFSS and the meandered structure obtained after squeezing the dipole. The red part in the tag design is the input port.

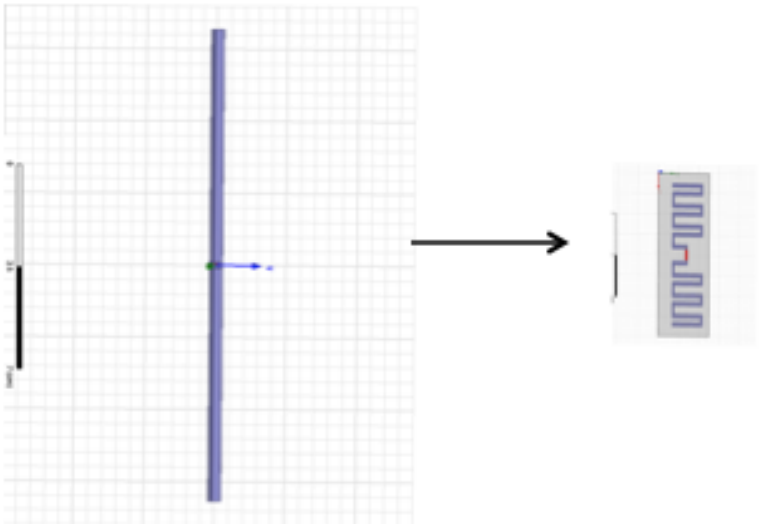

Figure 2.4: Half-wave dipole before and after squeezing

2.2 Design Goals

Table 2.1 lists the design goals for the work done in this thesis.

Table 2.1: Proposed design goals

Design Parameter	**Value**	**Justification**
Operating frequency	915 MHz	Unlicensed in the ISM band
Tag antenna dimensions	8×2 × .2cm	Common size for a tag
Tag antenna type	Electrically small	Antenna is electrically small
Operating wavelength	.3278 meters	$\lambda = \frac{c}{f}$
VSWR	≤ 2.5	Decent match
Bandwidth	40 MHz	Based on VSWR
Return loss	-10 dB	Low return loss at 915 MHz
Substrate	Single sided copper (FR4)	Easily available

2.3 Design Constraints and Trade-offs

Some tradeoffs are made in going from a simple dipole to a meandered structure as shown in Figure 2.4. The two most important tradeoffs are:

1)Low current
2)Low gain

Low current: Current in both arms of an ideal dipole is uniform and in the same direction. However, this is not true if you squeeze the dipole and have a meandered line structure as shown in Figure 2.4.

By squeezing the dipole, the current in adjacent meander lines will always be equal and opposite in direction. Figure 2.5 shows the equivalent current density (J) vector measured in amperes per meter.

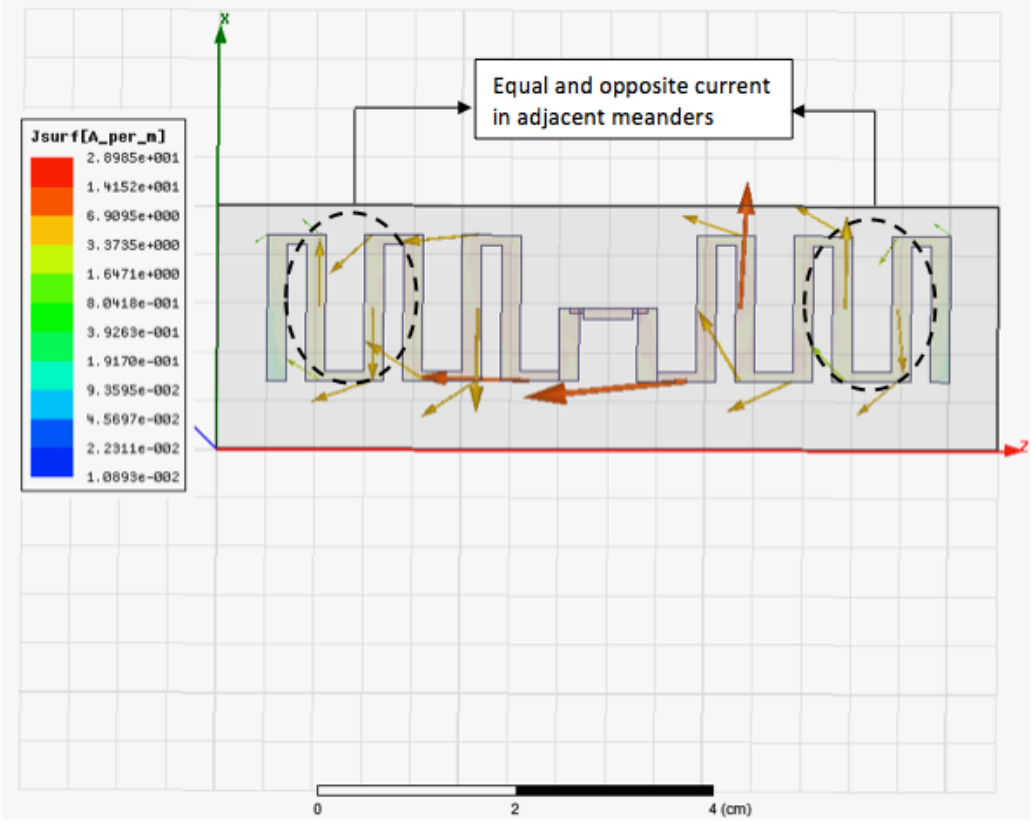

Figure 2.5: Equivalent current vector simulation in HFSS

From Figure 2.5 it can be seen that the current in adjacent meanders will always cancel out, hence the current contributing to the radiation efficiency will be only through the non-parallel meanders. Therefore, the radiation efficiency will go down.

Low gain: Gain is related to aperture size through (2.1)

$$G = \frac{4\pi A_{eff}}{\lambda^2} \tag{2.1}$$

where A_{eff} is the effective aperture size; the largest maximum physical area of an antenna.

By meandering the dipole, the largest possible dimension of the antenna was reduced and as a consequence the gain of the tag antenna will also go down as is shown in Chapter 7. Gain of an ideal half-wave dipole is 2.51 dB. Since the meandered line antenna structure is derived by squeezing a dipole hence the gain of the tag antenna will be less than 2.51 dB since the effective aperture size is reduced by squeezing the dipole.

Highly directive antennas are useful for point to point communication where the transmitter and the receiver are fixed. Dish antennas receiving signals from a geo-stationary satellite commonly have very high gain (10-40 dB) [4]. Lower gain is a favorable thing in this case. Common applications of RFID systems include asset tracking, access control and others as stated in Table 1.1. For most of these applications we don't know the angle from which we would be receiving the signals from the receiver. For example, a box which is being tracked should be able to pass through a reader from any angle and not necessarily a fixed angle. Thus having a low gain and an omnidirectional type radiation pattern is a favorable thing in this case.

2.4 Design Simulations

Figure 2.6 shows the design that was simulated in HFSS. Substrate was FR4 (Epoxy) with permittivity 4.4. Height of the substrate was 0.2 cm. All

meander lines were given electrical properties of copper. A radiation box approximately quarter wavelength from the center of the antenna was also simulated as shown in Figure 2.7.

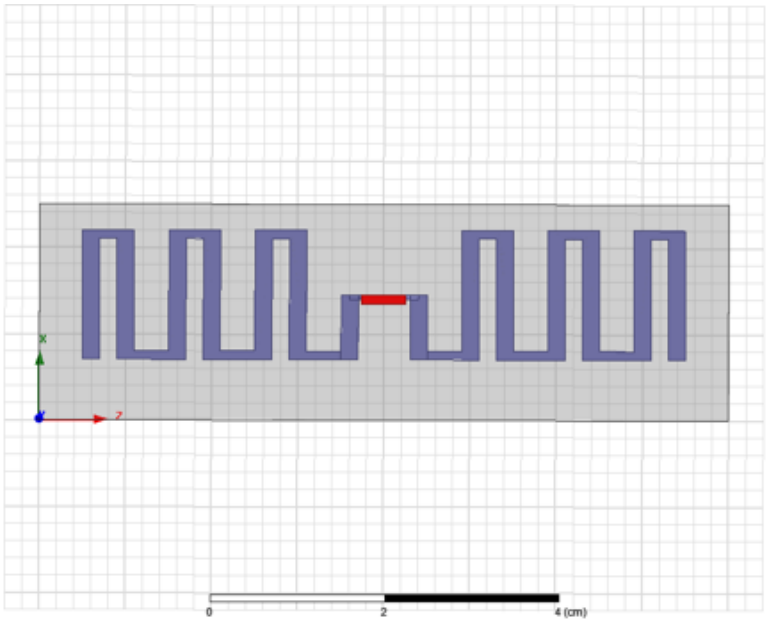

Figure 2.6: Tag antenna design in HFSS

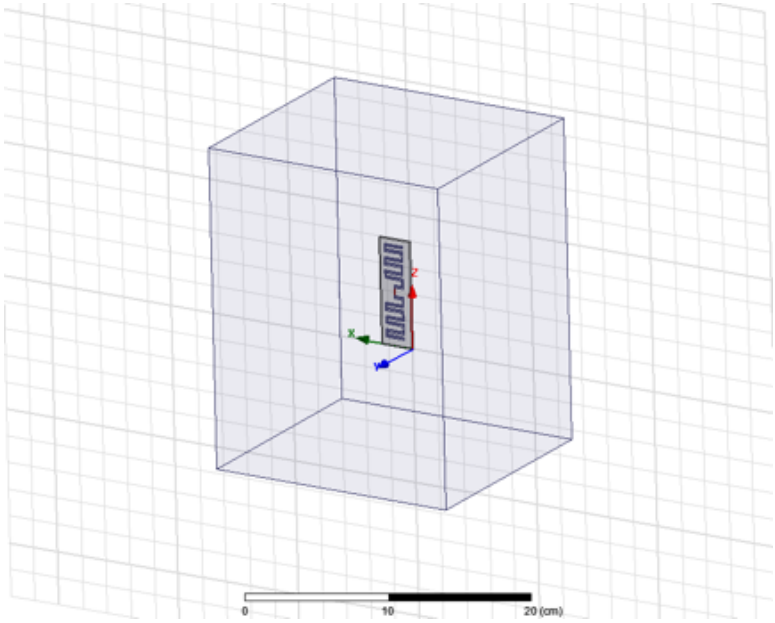

Figure 2.7: Radiation box

2.5 Design Optimization

Finding the right dimensions of the meander lines is not intuitive. A parameterized sweep was run in HFSS to find the dimensions best suiting the design goals and specifications.

To run a parameterized sweep, the height of the substrate, the width and the length of the meander lines were made as variables. For a small increase in these variables the corresponding changes in S_{11}, impedance and VSWR were investigated. The value of these variables which give the simulation results close to the design specifications were selected.

Figures 2.8 and 2.9 show the variation in simulation design during the parameterized sweep. Figure 2.8 shows the design with width of meanders as 0.1cm. Figure 2.9 shows the design with width of meanders as 0.2 cm.

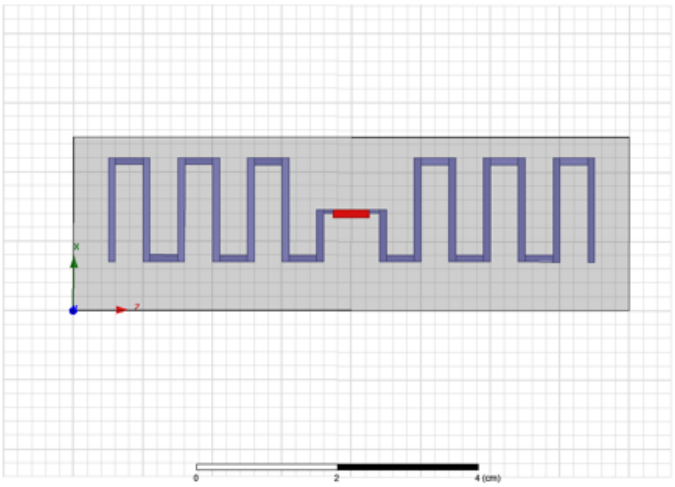

Figure 2.8: Design simulation with width of meanders as 0.1 cm

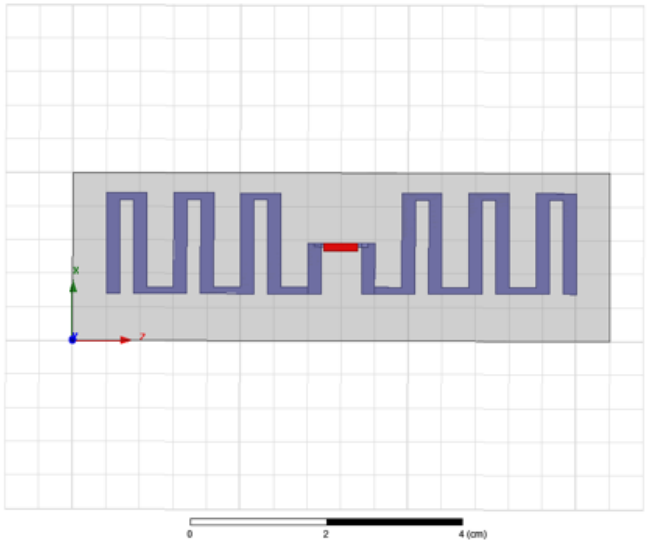

Figure 2.9: Design simulation with width of meanders as 0.2 cm

The width of the meander lines was varied from 0.1 to 0.2 cm in steps of 0.025 cm. Figure 2.10 shows the corresponding changes in the S11 and Figure 2.11 shows the corresponding changes in impedance for an increase in the width of the meanders from 0.1 to 0.2 cm in steps of 0.025 cm.

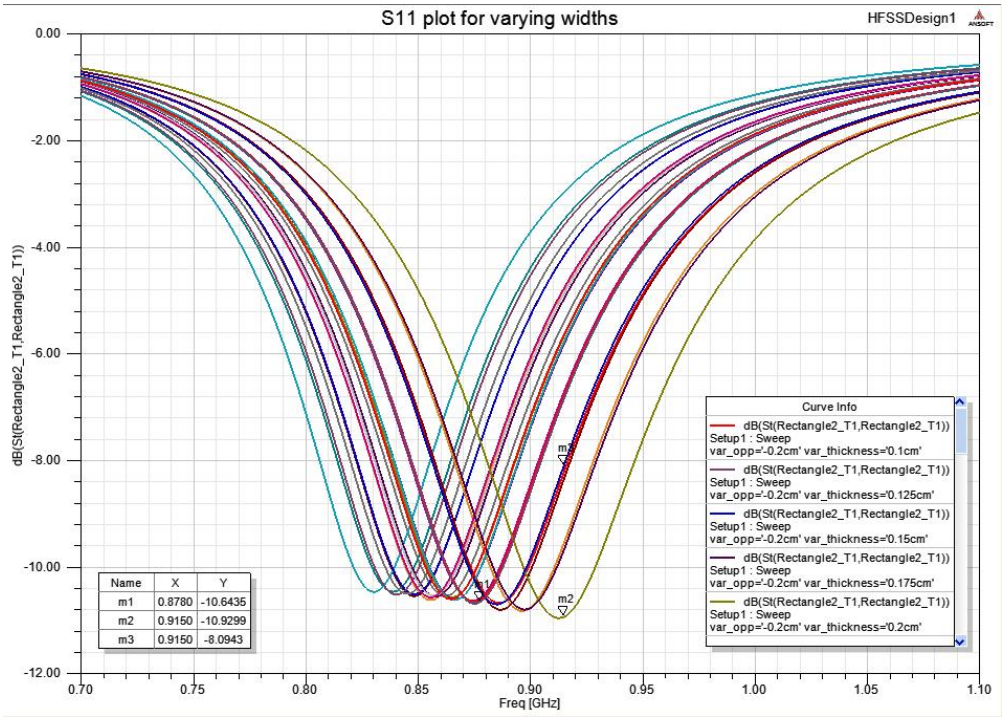

Figure 2.10: Parameterized S11 plot for varying width of meanders from 0.1 to 0.2 cm in steps of 0.025 cm

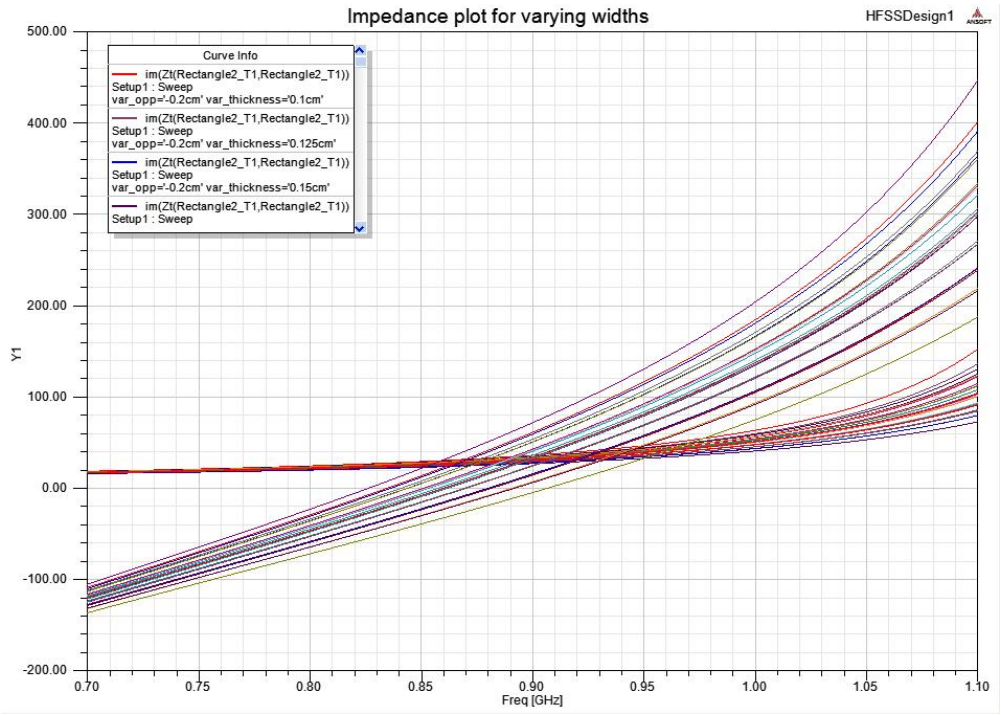

Figure 2.11: Parameterized impedance plot for varying width of meanders from 0.1 to 0.2 cm in steps of 0.025 cm

From Figure 2.10 it is clear that a width of 0.2 cm gives a return loss of about -10 dB which is close to the design goals as specified in Table 2.1 in Chapter 2. The impedance at 0.2 cm is also close to the design goal. A similar approach was taken to find the right dimension of the height of the meander and the height of the substrate. Figure 2.12 shows the final design dimensions of the tag antenna that was simulated in HFSS.

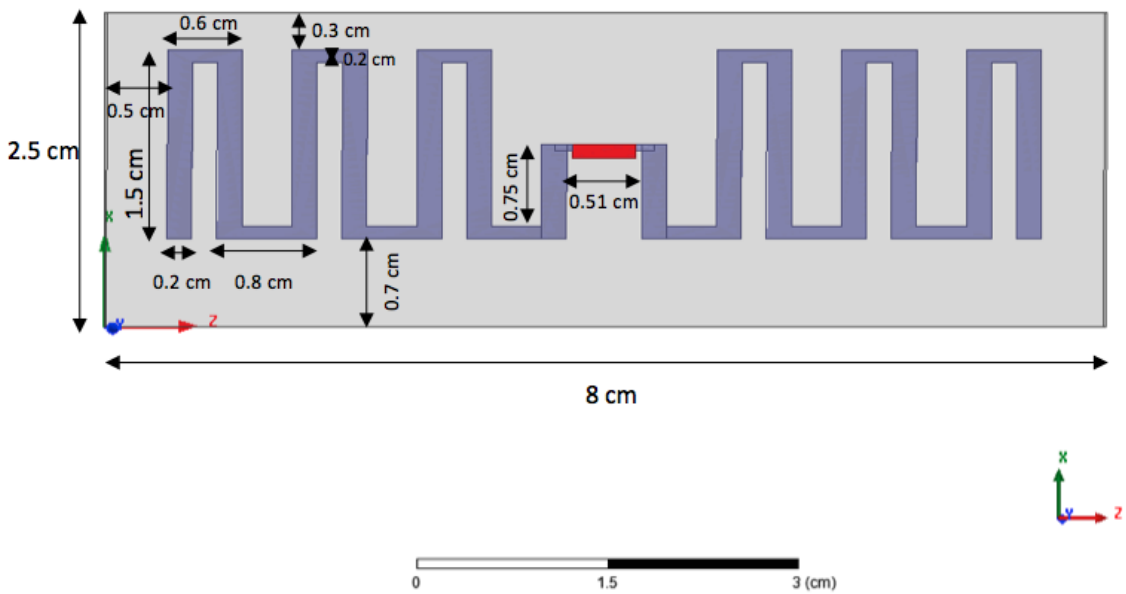

Figure 2.12: Dimensions of the tag antenna simulated in HFSS

CHAPTER 3

FABRICATION

This chapter describes the fabrication process of the antenna starting from the substrate to final design. It also highlights the problem faced during fabrication and methods used to solve them.

3.1 Fabricating the Antenna

A flow chart summarizing the fabrication process is shown in Figure 3.1

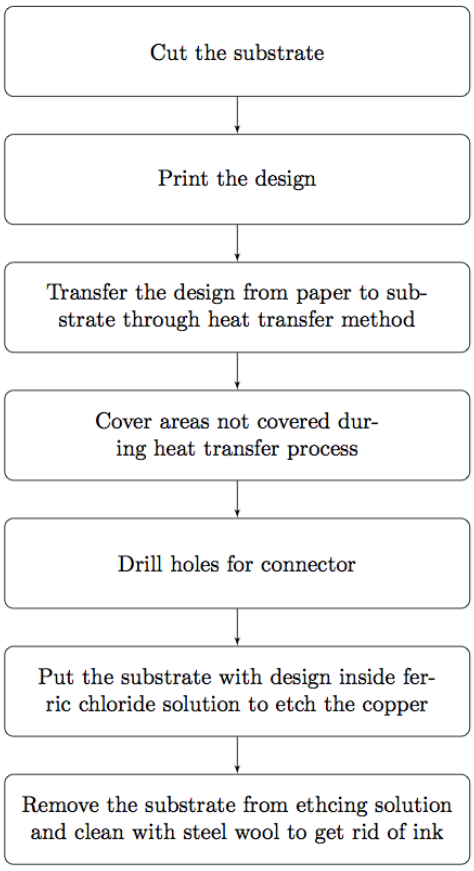

Figure 3.1: Flowchart summarizing the fabrication process

Each process in the fabrication process is described in detail below.

Step 1: Cut the substrate to match the antenna dimensions: Due to ease of availability, FR-4 was used as the substrate. The final tag design had length of 8 cm and width of 2.5 cm. Thus from the entire substrate a smaller portion corresponding to the tag antenna dimensions was cut using a commercial cutter as shown in Figure 3.2.

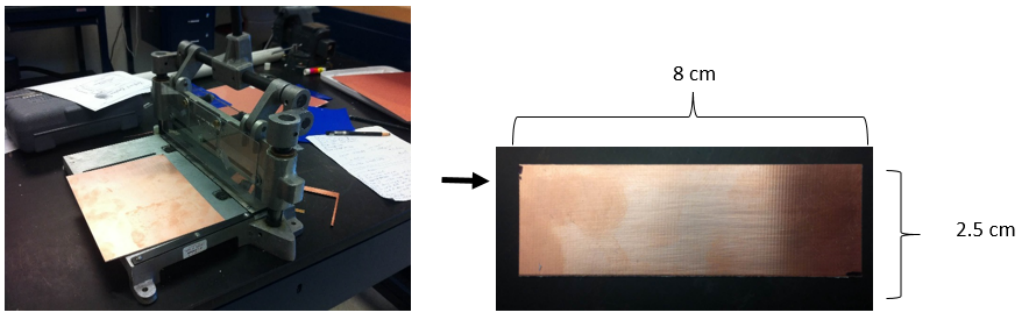

Figure 3.2: Cutting the substrate to match antenna dimensions using commercial cutter

Clean the substrate with steel wool to remove any polish: Any new dielectric board material comes with a shiny polish coated on it. This is done to make the product look more bright, shiny and better to solder and easier to etch. This polish was removed by cleaning the substrate with a steel wool as shown in Figure 3.3.

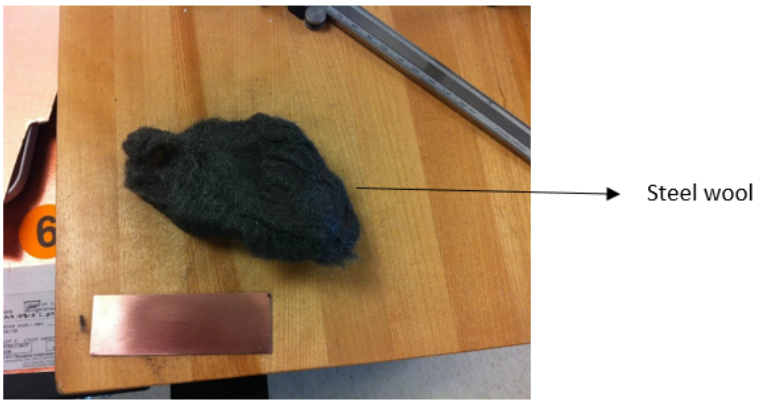

Figure 3.3: Steel wool used to remove any polish from the substrate

Step 2: Print the design of your antenna with exact dimensions on a PNP (press and peel) paper: After cutting the substrate to right dimension and removing any external polish, the design of the antenna was then printed on a press and peel (PNP) paper. To print the design with exact dimensions we can either draw the design with exact dimension in open office or we can simply copy the image from HFSS and paste it in paint. An important thing to keep in mind if one decides to use the HFSS and paint method is to make sure that the substrate is removed from the HFSS design and the copper is colored in black and white ink only. This is done because we want to print onto the pnp paper only in black color for easy transfer of design onto the substrate. Figure 3.4 shows the design printed on a PNP paper.

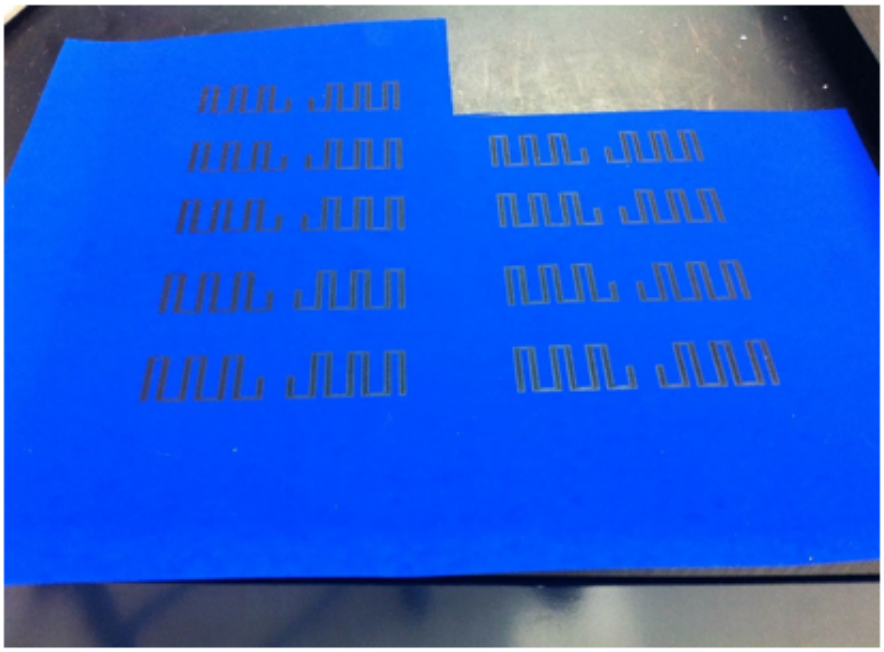

Figure 3.4: Printed antenna design on a PNP paper

Step 3: Transfer the design from paper to substrate through heat transfer method: After finishing step 3, the printed design on the PNP paper was put on top of the substrate and an iron was used to transfer the design from the PNP paper onto the substrate. Upon getting sufficient heat-the design pattern is transferred to the substrate. Figure 3.5 shows this step. Note: the iron has to touch the substrate and PNP paper.

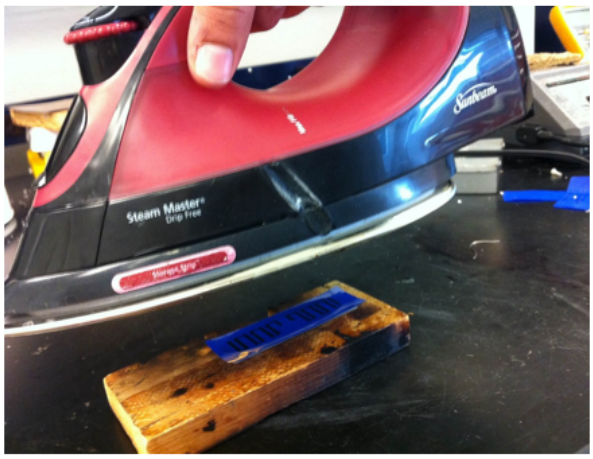

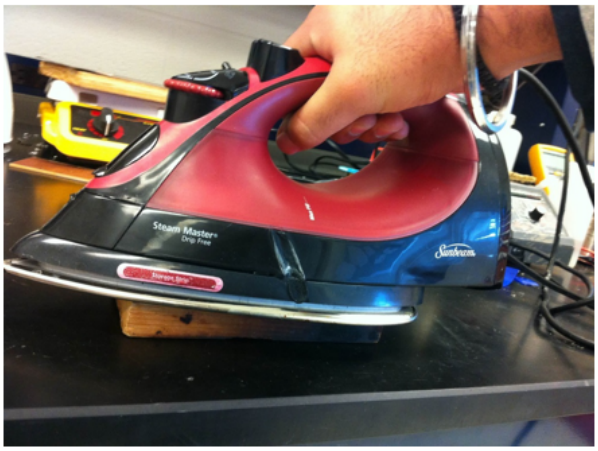

Figure 3.5: Iron used to transfer the design from paper to substrate by heat transfer

Step 4: Cover areas not covered during heat transfer process: After performing step 3, not all design was transferred to the substrate due to non-uniform supply of heat due to asymmetrical shape of the iron. To fix this, a thin black marker (Sharpie ^{TM}) was used to cover the areas where we wanted copper in our design as shown in figure 3.6.

Figure 3.6: Black marker used to cover the areas not fully covered during heat transfer process

Step 5: Drill holes for connector using drill press: Before etching, appropriate holes must be drilled for the connectors. For this design, the SMA connector was connected from the back side so we had to drill a hole through the substrate to connect to the SMA connector. Since the design of the antenna was symmetrical hence one half of the design was connected to the main conductor of the SMA and the other side to the outer conductor of the SMA. To do this three holes were drilled in total. One for inner conductor, one for outer conductor and one to hold the SMA connector in place. The dimension of the holes drilled were as follows:

Dimension of hole used to hold the SMA connector: 80 mil
Dimension of hole used to connect the inner conductor: 52 mil
Dimension of hole used to connect the outer conductor: 32 mil

All the holes were drilled through the drilling machine as shown in Figure 3.7.

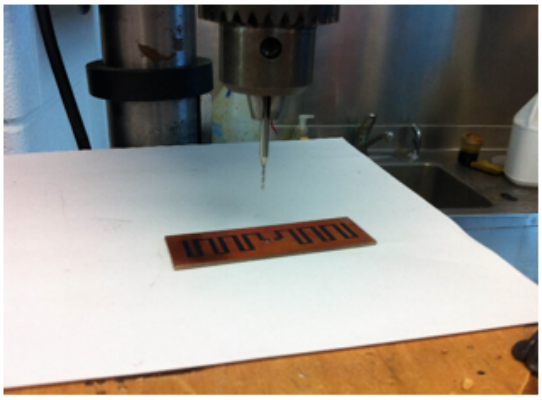

Figure 3.7: Drilling machine used to drill holes for connectors

Step 6: Put the substrate inside ferric chloride solution to etch copper: After drilling holes for the connectors and having adequate black ink in all the regions where we wanted copper, the substrate was then put in ferric chloride solution. The solution etches the copper from all the areas of the substrate where there is no black ink. This process usually requires to keep the substrate in solution for about 30 minutes.

Figure 3.8: Putting the substrate in ferric chloride solution to etch copper from the areas of substrate where it is not needed

Step 7: Remove the substrate from etching solution and clean with steel wool to get rid of ink: After about 30 minutes the substrate was removed from the solution and washed with water. Figure 3.9 shows the substrate after cleaning with water.

Figure 3.9: Substrate after removing from ferric chloride solution and rinsed with water

Even after rinsing it with water, the copper traces were not visible. All the traces were beneath the black ink of the marker used in step 4. Steel wool was again used to clean the marker and see the actual copper traces. Figure 3.10 shows the structure after removing the ink.

Figure 3.10: Substrate after removing the left over ink by cleaning it with steel wool

Figure 3.11 shows the actual fabricated antenna after soldering the all the connections.

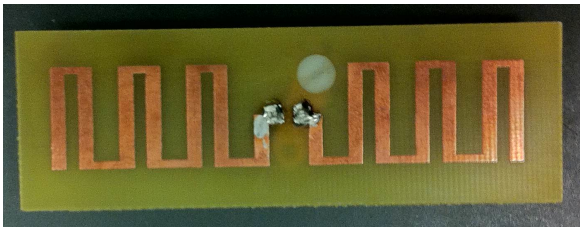

Figure 3.11: Final fabricated antenna after soldering all connections

3.2 Discrepencies during Fabrication

Even after etching the copper from the substrate, the actual design of the fabricated antenna was not exactly same as designed in simulations using HFSS. The meander lines in HFSS were straight, clear and with no discontinuities. This was not the case with the meandered lines of the fabricated antenna. Figure 3.12 below shows the fabricated antenna as seen under a microscope. Notice the zig-zag pattern. The black ink from the marker is also visible in the Figure 3.12.

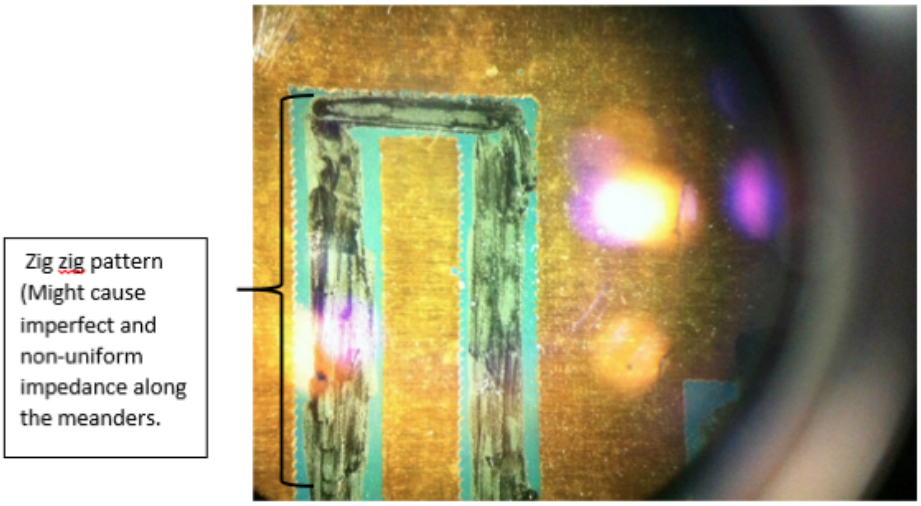

Figure 3.12: Fabricated antenna as seen under a microscope before putting in ferric chloride solution

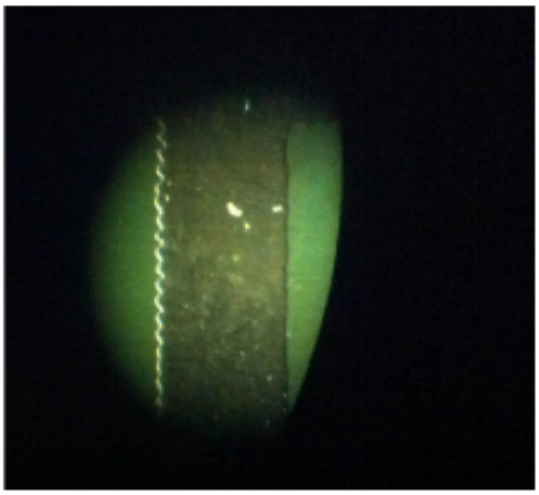

Figure 3.13: Fabricated antenna as seen under a microscope after removing from ferric chloride solution

A close investigation to the above seen zig zag pattern confirmed that these were coming from the printer as the printer that was used to print the antenna design could only print so many pixels or dots per inch (DPI). This was confirmed when we looked at the printed design on the PNP paper under a microscope. Figure 3.14 below shows the printed design on the PNP paper as viewed under a microscope.

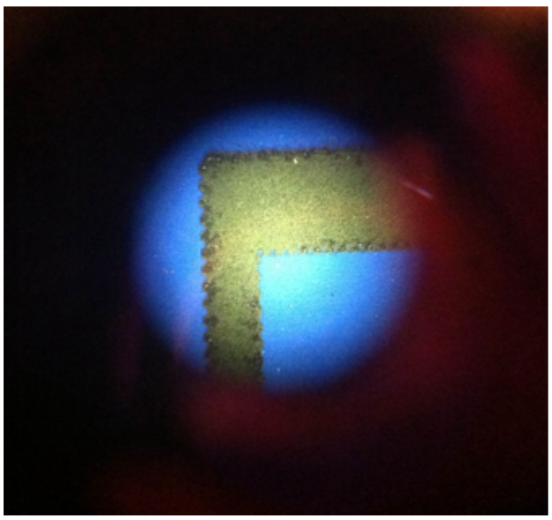

Figure 3.14: Printed antenna design on PNP paper as seen under a microscope

The only way to fix this discrepancy of zig zag print is by either using

a very high quality expensive printer or by manually drawing lines with a ruler and a marker. The latter takes long time as you have to look under the microscope for each zig zag and carefully draw a line to fill the zig zag pattern with a straight line. There is another way to fix this discrepancy and that is by using the milling machine to remove the copper.

CHAPTER 4

BALUNS

Balun comes from two words - **Bal**anced and **Un**balanced. A balun is used to balance an unbalanced transmission line. The need for a balun comes from the fact that for a dipole, ideally we want the current in the both arms to be equal. Since a dipole is connected to a coaxial cable, achieving this can sometimes be a challenge. The following section describes the need for balun and what causes the current to be unbalanced in some common transmission lines. This chapter also highlights the working principle of a bazooka balun which was used in this thesis.

4.1 Need for Balun

Some common types of transmission lines are:
1) Coaxial cable
2) Microstrip
3) Stripline
4) Balanced lines

Table 4.1 gives the main difference between the types of transmission lines.

Table 4.1: Main differences between types of transmission lines

Type of transmission line	Balanced
Coaxial cable	No
Microstrip	No
Stripline	No
Balanced lines	Yes

A coaxial cable or simple a co-ax is one of the most common cables used for RF. The problem of connecting a co-ax directly to a dipole antenna is that it is unbalanced. Consider Figure 4.1:

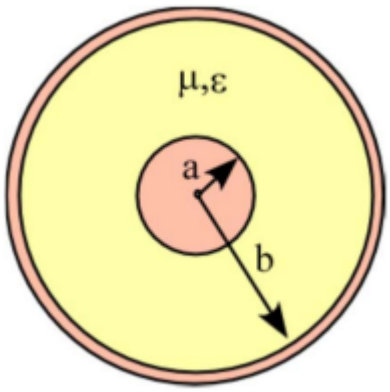

Figure 4.1: Top view of a co-ax cable

A co-ax cable has two conductors. One inner conductor and one outer conductor. Inner conductor has a radius "a" while the outer conductor has radius "b". For every co-ax, b>a. Since the radii of both the inner and outer conductor is different, hence the current density (J) is different for both the conductors. This difference in current density between the inner and outer conductor causes an unbalance and hence if the antenna is not matched properly, the coax cable also tends to radiate apart from the antenna and causes discrepancies in measurement results.

If we feed a balanced antenna structure with an unbalanced feed line, then we get some unwanted current called as the common mode current which arises due to this mismatch between the balanced and the unbalanced line. These common mode currents travel back down the coax and radiate and thus the coax cable also becomes a part of our antenna and radiates. Even though a coax causes unbalancing problem it is still widely used because of its low cost.While taking measurements for balanced antenna structure a balun should always be used. Specially when working with electrically small antennas.

4.2 Bazooka Balun

To better understand the need for balun, consider Figure 4.2:

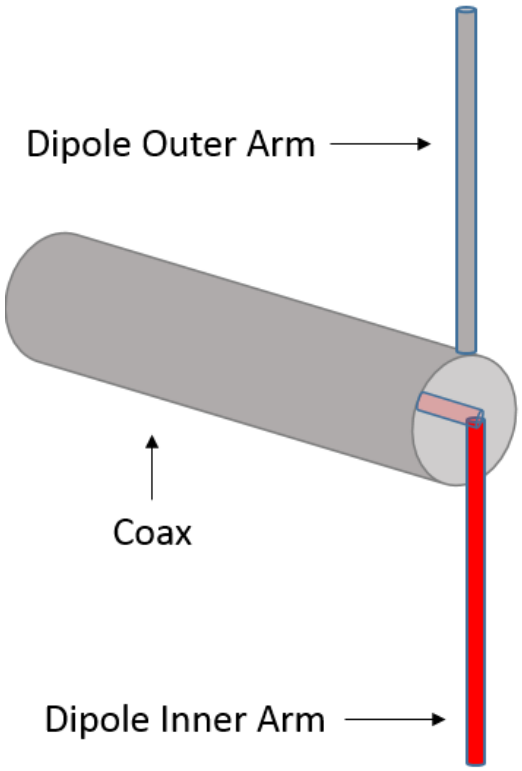

Figure 4.2: Pictorial representation of a dipole connected to a coaxial cable

Figure 4.2 shows how a dipole is connected to a coax. Since a dipole is balanced antenna structure hence we want the current going into the dipole to be balanced. However, since the dipole is fed through a coax cable which is an unbalanced transmission line hence we get unwanted currents and thus apart from the dipole the coax also radiates and causes discrepancies in measurement results.

Figure 4.3 shows the current distribution on the dipole. Ideally, we want I_a to be equal to I_b. However, as described above since the outer conductor of the coax has a different current density than the inner hence an unwanted current I_c flows on the outer conductor opposite to the direction of I_b as shown in Figure 4.3.

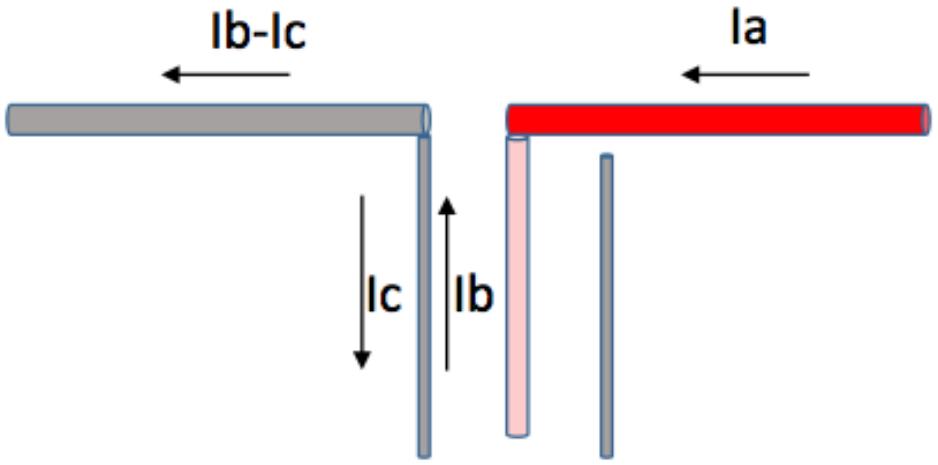

Figure 4.3: Equivalent current distribution on a dipole when connected through a co-ax [4]

I_c is called the common mode current. We want I_c to be equal to zero. This is achieved by introducing a sleeve or a bazooke around the outer conductor. The length of the sleeve should be quarter wavelength. The farther end of the sleeve has to be a short because quarter wavelength from a short is an open where the impedance is infinite and current is zero. Since the current on the bazooka or the sleeve is zero hence equal and opposite current I_c also has to be zero. Hence we get Ic to be equal to zero. This process is called as choking the common mode current I_c.

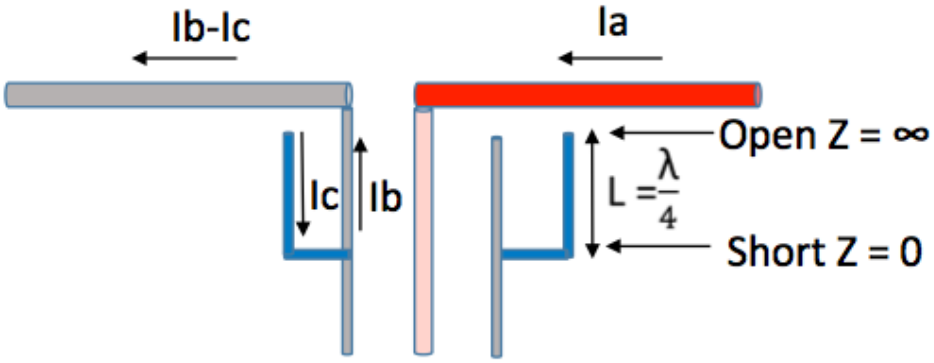

Figure 4.4: Quarter-wavelength sleeve around a coax

Figure 4.5 shows the model for the balun. Figure 4.6 shows the balun that was used for taking measurements.

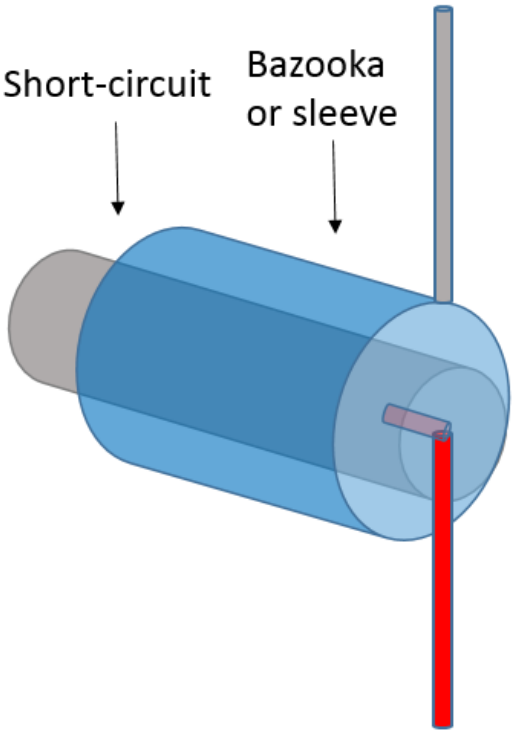

Figure 4.5: Model for bazooka balun

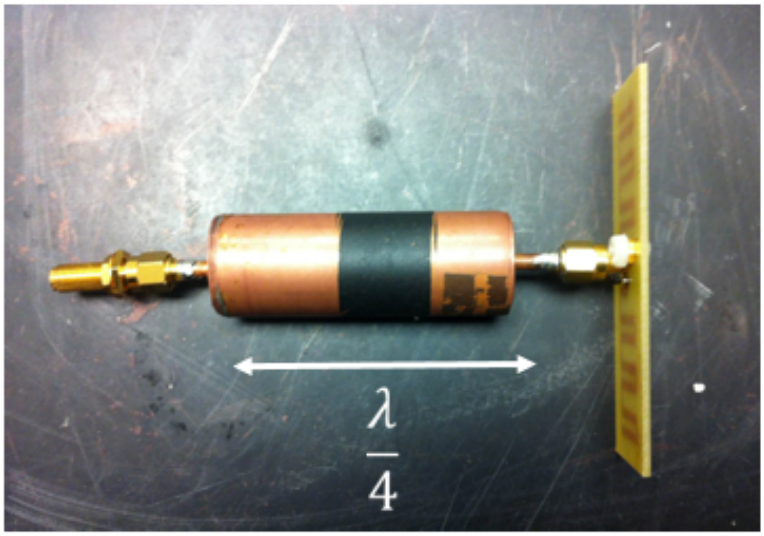

Figure 4.6: Bazooka balun used for taking measurements

CHAPTER 5

MEASUREMENT PROCESS

This chapter describes the measurement setup and the measurement process. Radiation pattern measurements were taken inside an anechoic chamber in the antenna lab at University of Illinois at Urbana-Champaign. All other measurements were done through a standard VNA, signal generator, signal analyzer and standard RF cables.

5.1 Radiaton Pattern Measurements

Radiation pattern of any antenna is measured in a closed, isolated and a non-echoic room. Such rooms are called anechoic chambers (an-echoic meaning no echo). An anechoic chamber as described in [7] is a room designed to completely absorb reflections of sound or electromagnetic waves. They are also insulated from exterior sources of noise. Anything radiated from a source inside an anechoic chamber does not experience multi path or reflections. This is because the interior of an anechoic chamber is made of special cones made from foam dipped in carbon to absorb the reflected waves. Once the waves are radiated, they hit the cones and get absorbed.

5.2 Test Measurement Procedure

Figure 5.1 summarizes the test measurement process:

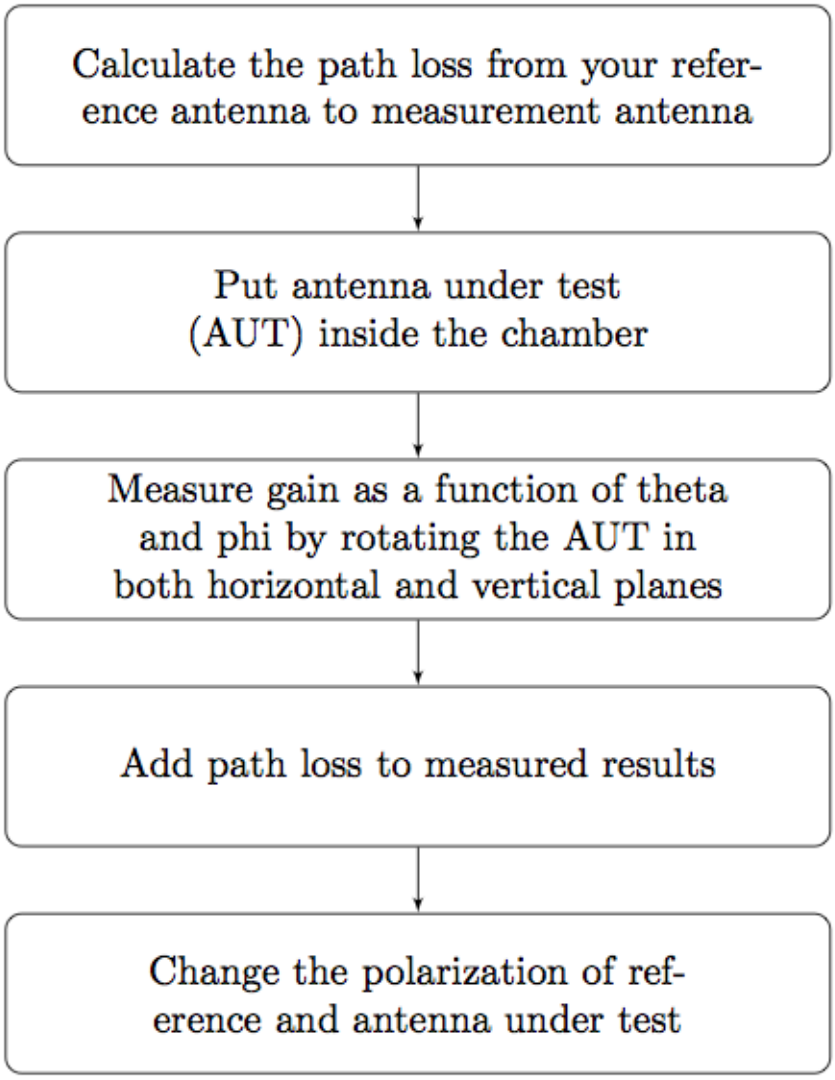

Figure 5.1: Flow chart summarizing the measurement process

The steps in the flowchart are explained in detail below.

Step 1: Calculating the the path loss from reference antenna to measurement antenna: First step in taking any RF measurement inside a chamber is to calibrate and calculate the path loss due to air, cables involved in the measurement system.

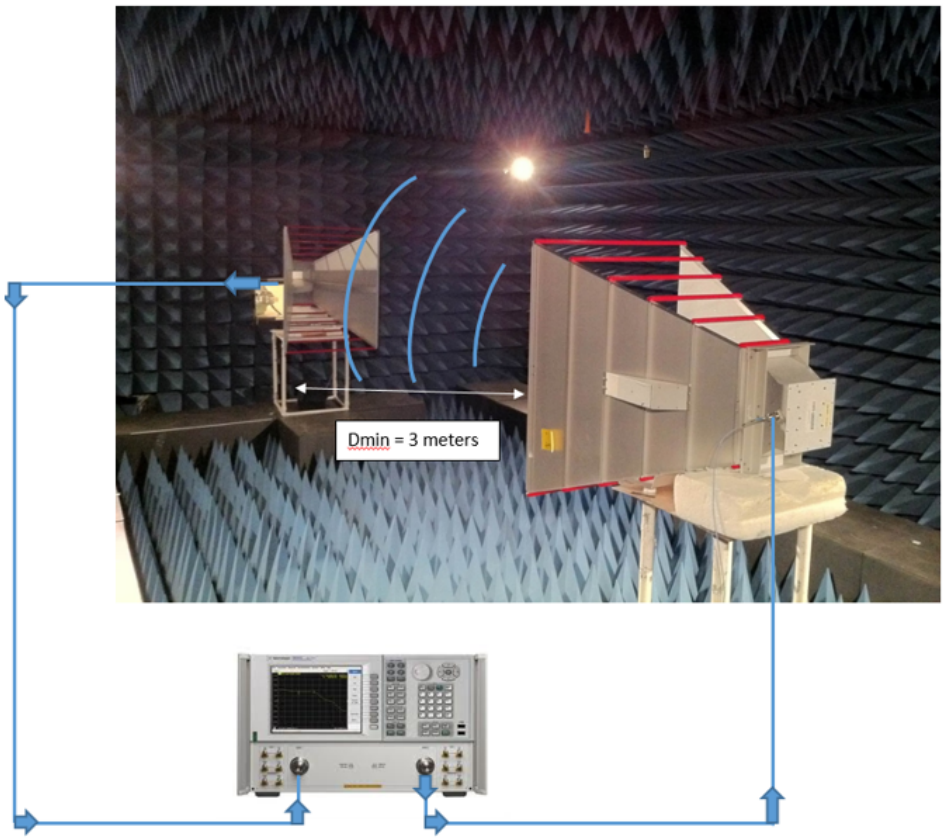

Figure 5.2: Path loss calibration setup

Two standard horn antennas were used as shown in the Figure 5.2. The standard gain of these horn antennas is around 9 dBi at 915 MHz [8]. The distance between them is about 3 meters which is more than the Fraunhofer distance where we can assume spherical electromagnetic waves to be planer waves. One horn antenna acts as transmitting antenna while the other acts as receiving. Since we know the gain of both these antennas, we do a 2-port S_{21} measurement to calculate the path loss using friis transmission formula

$$\frac{P_r}{P_t} = \frac{G(tx)G(rx)\lambda^2}{(4\pi D)^2} \tag{5.1}$$

where

$\frac{P_r}{P_t}$ is the S_{21} which is measured from the VNA.

G(tx) is the gain of the transmitting antenna (9 dBi).

G(rx) is the gain of the receiving antenna (9 dBi).

$\frac{\lambda^2}{(4\pi D)^2}$is the path loss.

Taking log on both sides of (5.1) we get:

$$S_{21}(dB) = G(tx) + G(rx) - path\ loss \tag{5.2}$$

Transmitting antenna was connected to port 2 of the VNA. Receiving antenna connected to port 1. Thus S_{21} gave the transmission from port 2 to 1. Standard gain of horn antenna used were 9 dBi each.
Putting these numbers in equation 5.2 we get path loss as

-3.4 (dB) = 9(dBi) + 9(dBi) - path loss

Hence, path loss = 21.4 dB

Note: This path loss was computed without the balun attached to transmitting antenna. In our measurement setup for measuring the radiation pattern of fabricated antenna we used a balun to connect the coax to the antenna. Thus we would have additional mismatch loss which are taken into account in appendix A.

Step 2 and 3: Replacing the standard horn antenna used for transmitting with our fabricated RFID antenna. To calculate the gain we again use (5.1) but this time the unknown in (5.1) is the gain of our AUT.

First the gain measurement in theta (horizontal) plane was recorded, thus the AUT was connected in the following way

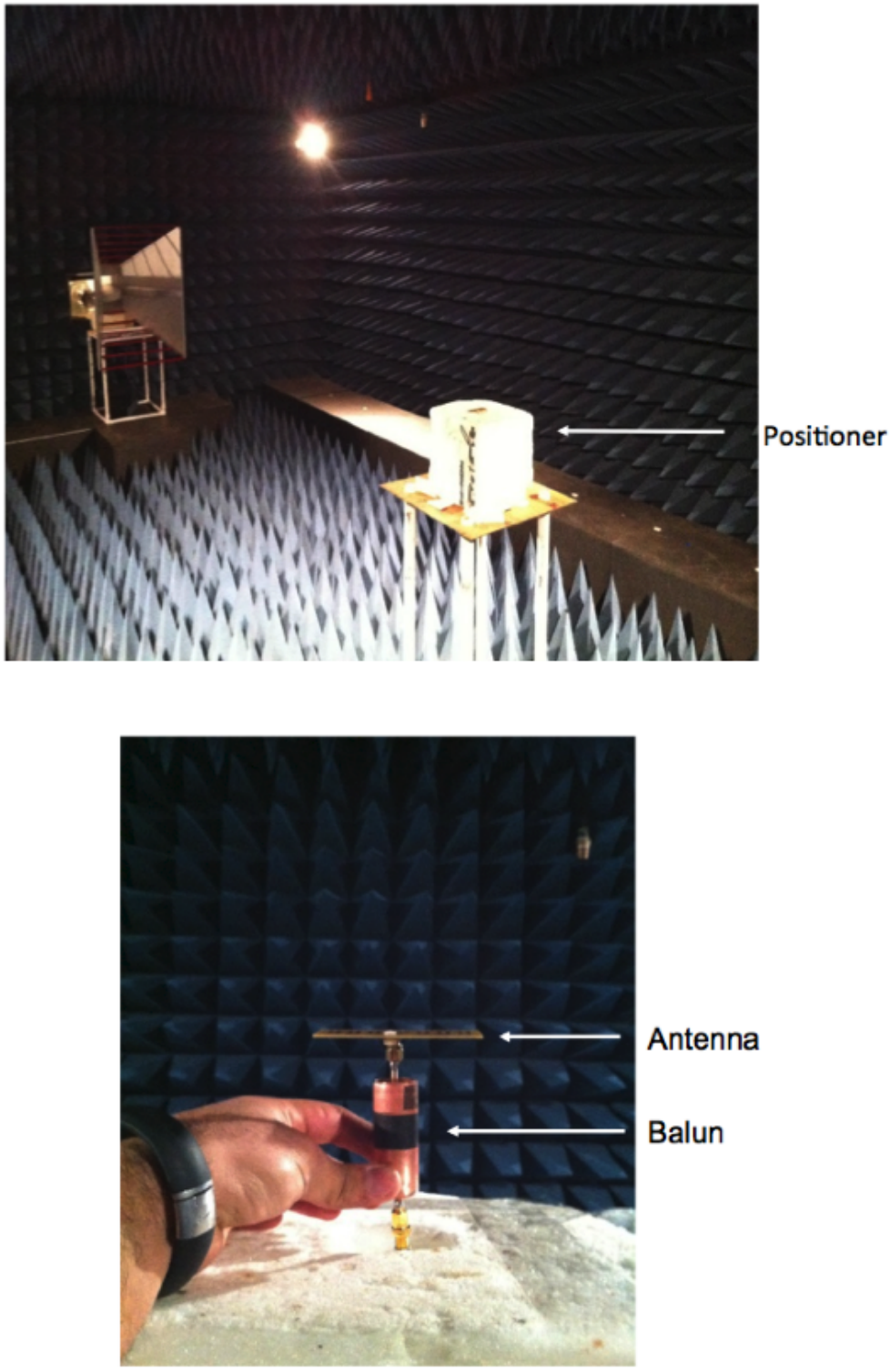

Figure 5.3: Antenna setup for calculating the gain as a function of theta

2 port S_{21} measurement was recorded with the AUT rotating from 0 to 360 degrees to get the full theta pattern. From 5.3 we have

$$S_{21}(dB) = G(tx) + G(rx) - path\ loss \tag{5.3}$$

where,

$S_{21}$is measured from the VNA at each angle of rotation of AUT.

G(tx) is the gain of the AUT (unknown).

G(rx) is the gain of the receiving antenna (9 dBi).

Path loss is 21.4 dB (calculated from step 1 above).

Since S_{21}, G(rx) and the path loss is known, hence we get the gain values as a function of theta (from 0:360) using the above equations.

Step 5: Changing the polarization of AUT and the reference antenna: To take radiation pattern measurements in the phi plane we rotate the AUT and the reference antenna by 90 degrees as shown in Figure 5.4.

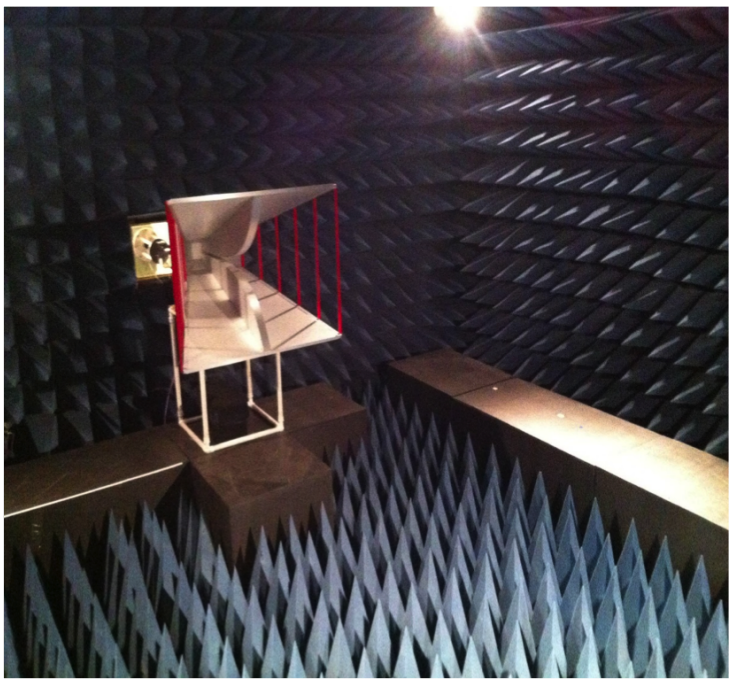

Figure 5.4: Vertically polarized horn antenna for phi plane measurements

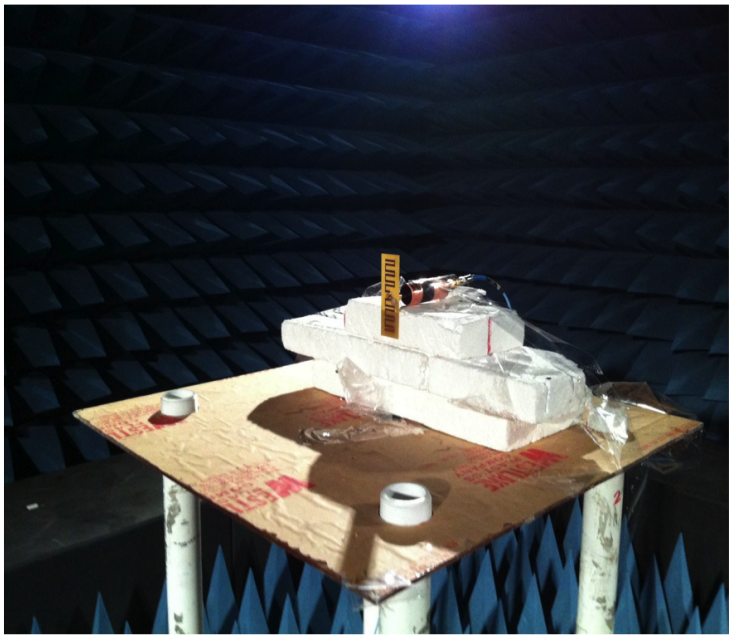

Figure 5.5: Vertically polarized AUT for phi plane measurements

To get the phi plane measurement same formula and calculations which were used for theta plane are used.

5.3 Measurements from the VNA

Radiation pattern measurements were taken inside the chamber. Some other performance parameters such as S_{11}, VSWR, and Impedance were measured by using the VNA. Before taking VNA measurements, the VNA was calibrated by using a standard 1-port calibration kit with a standard short, open and load.

Note: The VNA was calibrated at the input of the balun. This was done to insure balanced current goes to the antenna while taking measurements. Hence the standard calibration standards were attached at the input of the balun and the balun was connected to the coax cable coming out of port 1 of the VNA as shown in Figure 5.6:

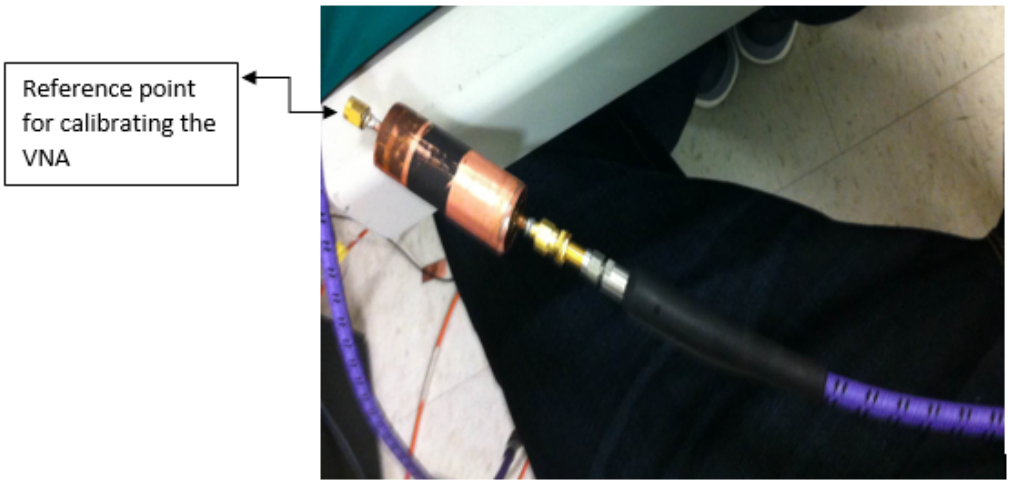

Figure 5.6: Reference point for calibrating the VNA

After calibrating the VNA, standard one port S-parameter measurement was done to observe the S_{11}, Smith Chart and VSWR performance of the fabricated antenna. All the measurement results are described in the next chapter.

CHAPTER 6

MEASURED VS. SIMULATED RESULTS

This chapter describes the comparison between the measured and the simulated results. All measured results are in blue and all simulated results are in red. All simulations were run in HFSS [9]. Radiation pattern measurements were taken inside an anechoic chamber in the antenna lab at University of Illinois at Urbana-Champaign. All other measurements were done through a standard VNA, signal generator, signal analyzer and standard RF cables.

6.1 S_{11} Comparison

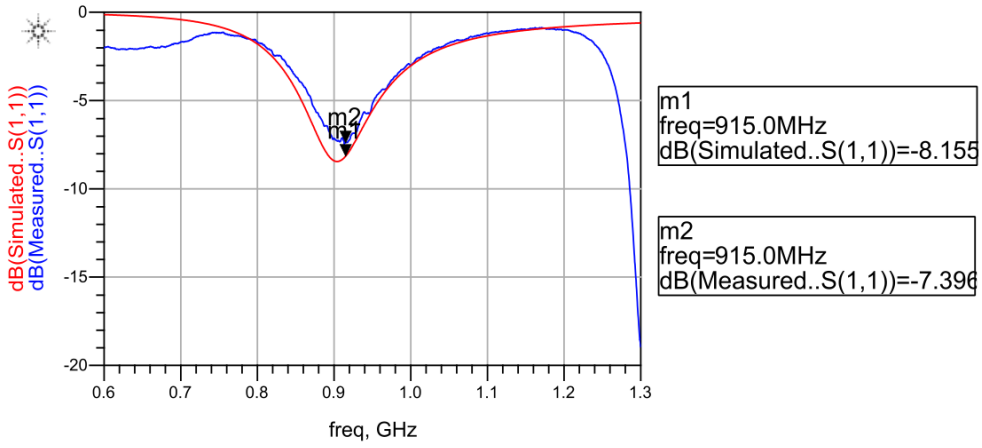

Figure 6.1: S_{11} comparison between measured and simulated results

S_{11} simulated was recorded as -8.155 dB whereas S_{11} of the fabricated antenna was observed to be -7.396 dB. The error between simulated and measured is less than one dB.

6.2 Impedance Comparison

6.2.1 Real(Impedance) Comparison

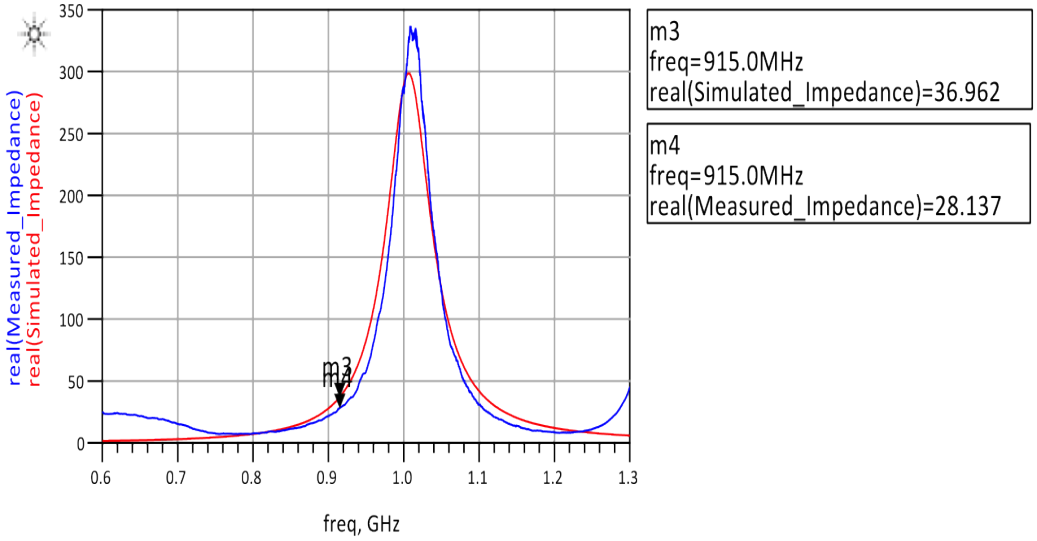

Figure 6.2: Real impedance comparison between measured and simulated results

6.2.2 Imaginary(Impedance) Comparison

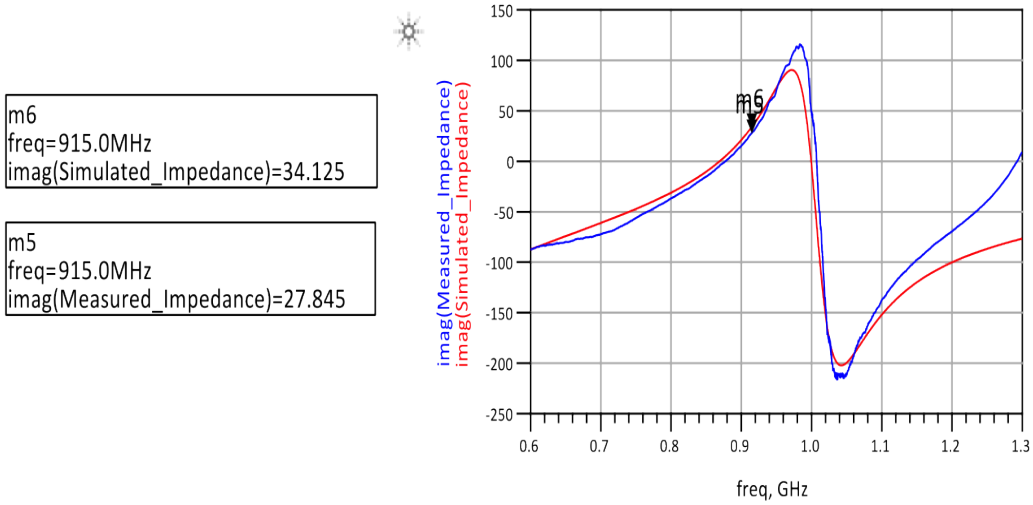

Figure 6.3: Imaginary impedance comparison between measured and simulated results

6.3 Smith Chart Comparison

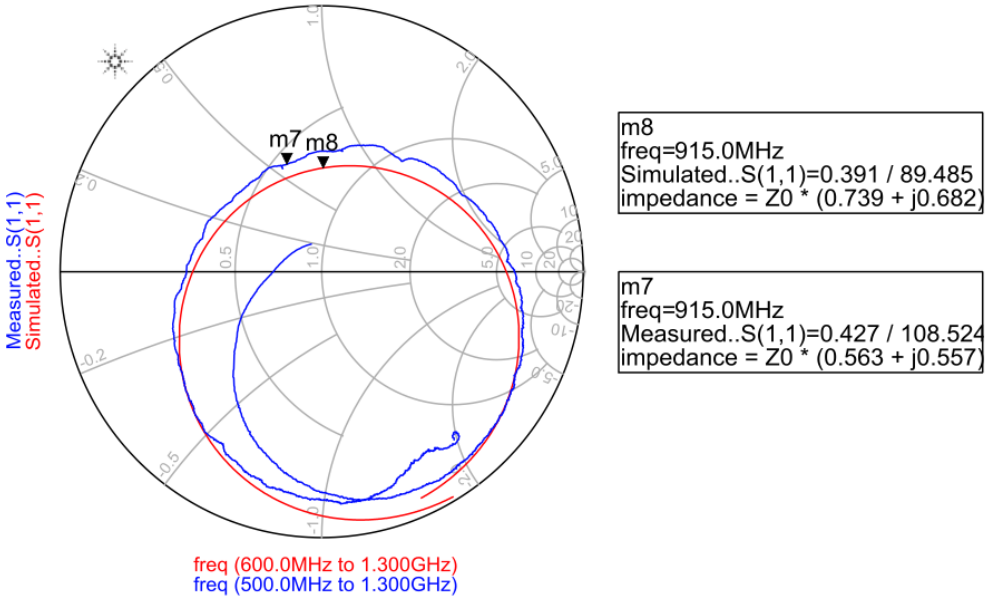

Figure 6.4: Smith chart comparison between measured and simulated results

From Figure 6.4 it is clear that on the Smith Chart both the simulations and the measured results start from about the same point, but as we go higher in frequency the measured results show some parasitics effects as the impedance becomes more capacitive and eventually becomes inductive.

This could be coming from the wire connecting the SMA connector to the antenna. The SMA connector and the wire connecting the SMA connector to the antenna were not modeled in the simulations, hence at higher frequencies we observe the parasitic effects coming from that wire which causes the measured results to be more capacitive and eventually inductive as compared to the simulated results.

6.4 VSWR Comparison

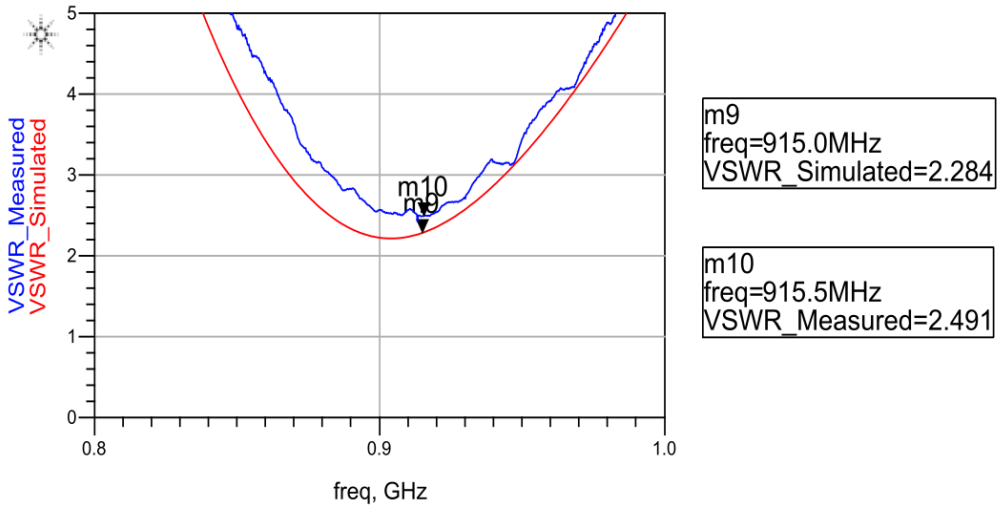

Figure 6.5: VSWR comparison between measured and simulated results

The measured VSWR was observed to be 2.491. Using (6.1) we can calculate the reflection coefficient as follows:

$$\Gamma = \frac{VSWR - 1}{VSWR + 1} = \frac{2.491 - 1}{2.491 + 1} = 0.43 \tag{6.1}$$

$$Returnloss = -20\log(\Gamma) = -20\log(0.42) = +7.39 \tag{6.2}$$

We can also compute the percentage of power reflected from the antenna. This would simply be

$$100 \times \Gamma^2 = 18.2\% \tag{6.3}$$

Thus 18.2 % of the input power will always be reflected from the tag antenna. In a similar way we can compute the power delivered to the antenna. This would be

$$100 \times (1 - \Gamma^2) = 81.51\% \tag{6.4}$$

Mismatch loss in dB would thus be

$$10\log(1 - \Gamma^2) = 0.87\,\text{dB} \tag{6.5}$$

6.5 Gain-Theta Comparison

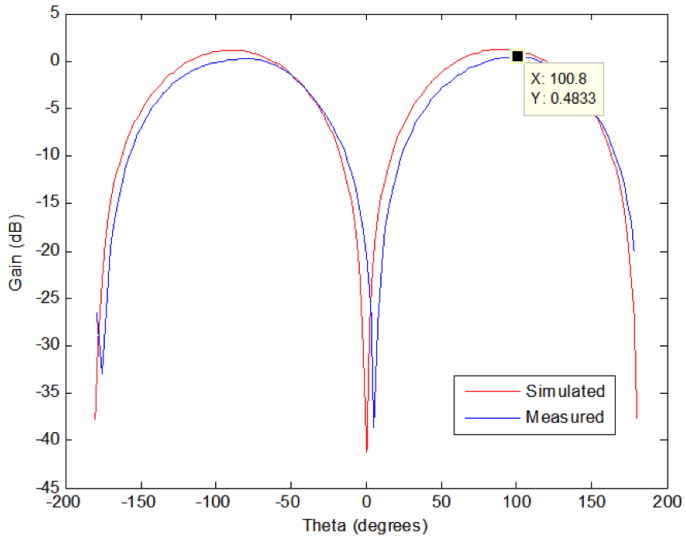

Figure 6.6: Gain comparison for theta plane in linear scale between measured and simulated results

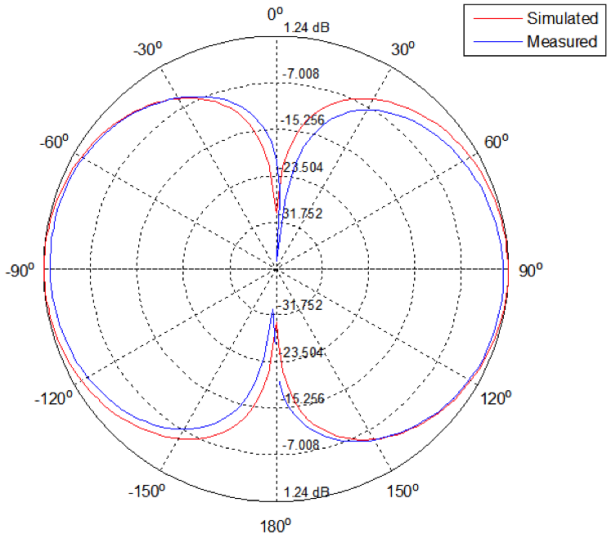

Figure 6.7: Gain comparison for theta plane in polar logarithmic scale between measured and simulated results

From Figure 6.6 it can be seen that the gain of the measured antenna is maximum for theta equal to 100° and the value is 0.4833 dB. The gain of a half wave dipole is 2.51 dB. Since the design of the tag is basically derived by squeezing a dipole hence we would expect the gain to be less than 2.51 dB since the effective aperture size is reduced as explained in chapter 2. The gain of a dipole is maximum in broadside side direction where theta is 90°. The gain of the tag was maximum at 100°. A shift of 10° is expected due to chamber errors.

For RFID application the gain of the tag antenna should be less since we do not know where the wave from the reader antenna is coming from. The tag antenna can be oriented in any direction. Hence having a lower gain and an omnidirectional type pattern is a favorable thing in this case.

6.6 Gain-Phi Comparison

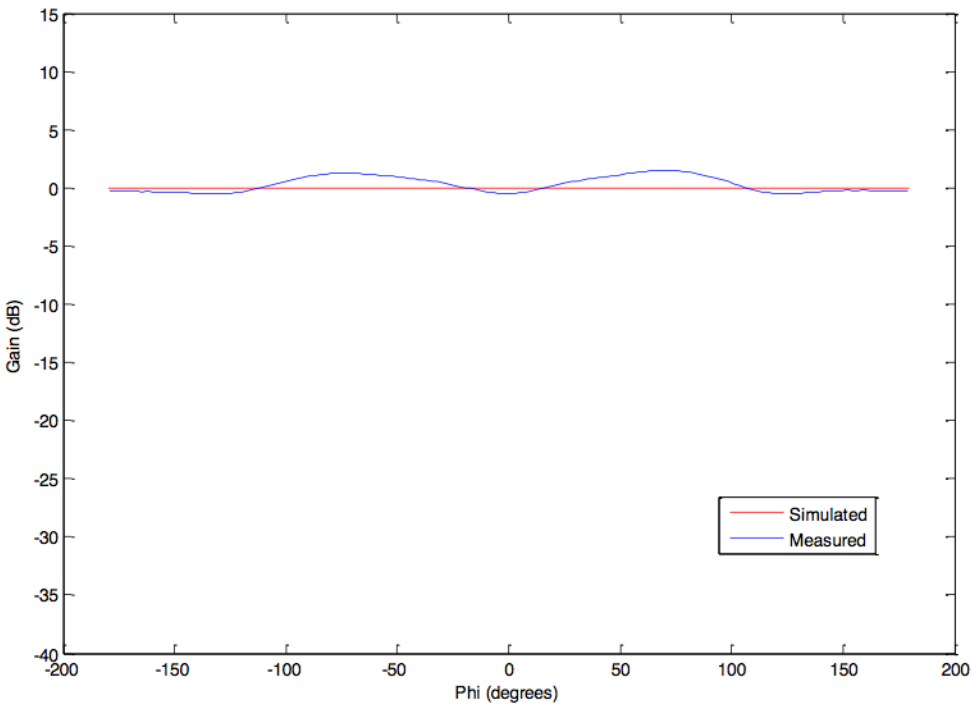

Figure 6.8: Gain comparison for phi plane in linear scale between measured and simulated results

Gain for phi plane is constant. This is what we expect since even for a

dipole, there is no phi-dependence on the radiation pattern. There are some slight variations in the phi-dependence which could be coming from chamber measurement error.

CONCLUSION AND FURTHER WORK

Conclusion

The fabricated antenna achieves a return loss of 7.39 dB, bandwidth of 40 MHz, VSWR of 2.4, input impedance of $28 + j27\,\Omega$ and a maximum gain of 0.488 dB. All these parameters match well with the design goals as specified in Table 2.1 of Chapter 2.

The work done in this thesis also highlights the problem of measuring radiation performance of balanced antenna structures with an unbalanced transmission line such as a co-ax. To get accurate measurements a balun should always be used.

While modeling the antenna in a simulation software, the exact model with all the connectors and all the wires should always be simulated. The SMA connector and the balun were not modeled in the simulations. The effect of this was observed since the measured and observed results were off by a big margin at first. Appendix B discusses how the effect of SMA connector was taken into account without modeling it in HFSS.

While taking radiation pattern measurements, the balun was attached to a 50 ohm co-ax cable whereas while calibrating and calculating the path loss, the horn antenna was matched to the same 50 ohm co-ax cable. The mismatch loss due to different impedance of the balun and of the cable is discussed in Appendix A.

Further work

Common RFIC chips have high capacitive impedance [10]. To have a good match the impedance of the RFIC chip should be conjugately matched to

the input impedance of the tag antenna. Further work can be done to get a better match and a low VSWR.

The tag antenna fabricated in this thesis used FR-4 as the substrate. Since the tags are generally attached to objects of different material properties, hence the effect of using a more flexible substrate and the effects on radiation pattern when the tag is attached to different materials can be investigated in the future.

APPENDIX A

MISMATCH CALCULATIONS

The impedance of (antenna + balun) was measured to be $26.6 + j23.95\,\Omega$. While taking radiation pattern measurements-the antenna along with balun was connected to a coax with standard $50\,\Omega$ impedance. This impedance mismatch loss would be extra apart from the path loss since the standard horn antenna used for calculating the path loss in Step 1 of Chapter 5 was matched to the $50\,\Omega$ impedance of the coax.

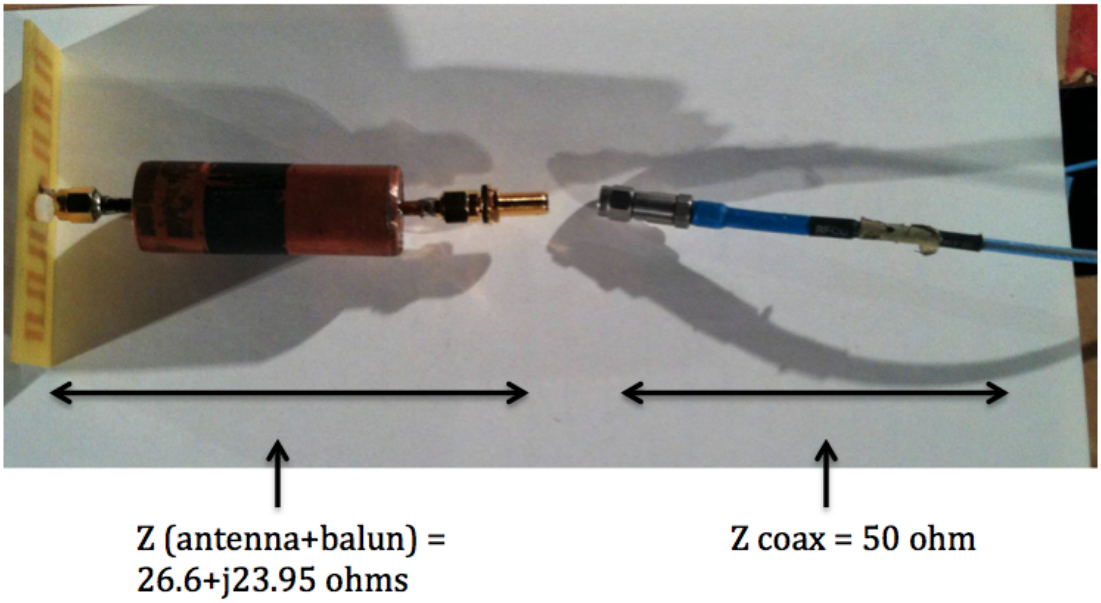

Figure A.1: Mismatch between impedance of (antenna+balun) and coax cable

$$\text{Mismatch loss} = \frac{4R_S R_L}{(R_S + R_L)^2 + (X_S + X_L)^2} \tag{A.1}$$

where,

$R_S = 50\,\Omega$ (Impedance of coax cable)

$R_L = 26.6\,\Omega$ (Real impedance of antenna+balun)

$X_L = 23.95\,\Omega$ (Imaginary impedance of antenna+balun)

$X_S = 0$

Putting all these numbers in (A.1) we get mismatch loss as 0.8259. Converting that to dB we get:

$$\text{Mismatch loss in dB} = 20\log(0.8259) = -1.6611\,\text{dB}$$

Thus -1.6611 dB was added to (5.2) to account for the mismatch loss while taking radiation pattern measurements.

APPENDIX B

ACCOUNTING FOR THE CONNECTOR

The SMA connector and the wire used to connect the SMA connector to the antenna was not modeled in the simulations, because of which large variations between the simulated and measured results was observed at first. To account for the connector without modeling it in HFSS, the extra phase in S_{11} coming from the connector and the wire was calculated. Twice of that phase was then subtracted from the phase of S_{11} corresponding to all frequencies. All the post processing was done in ADS and MatLab. Figure B.1 shows the length of the connector and the wire used.

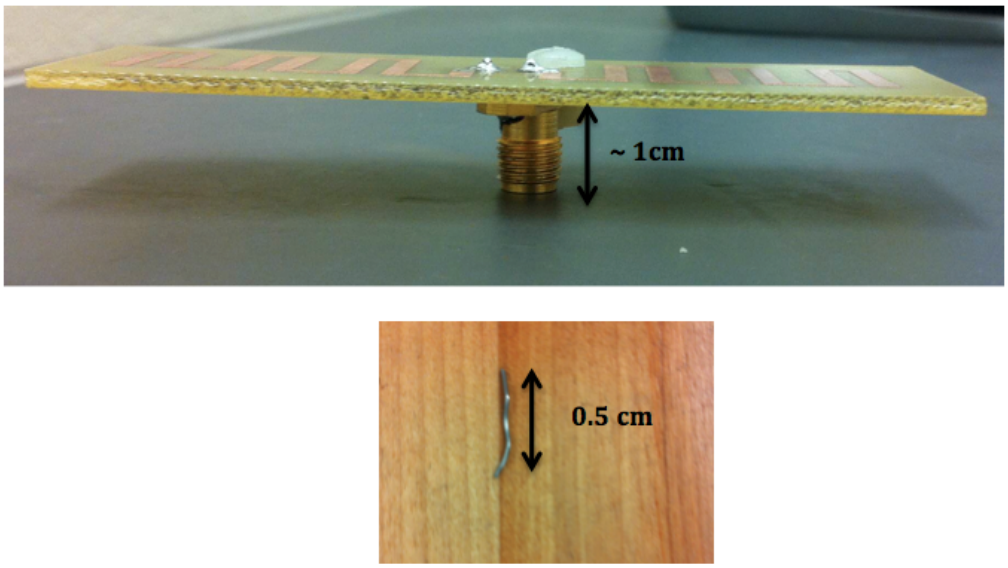

Figure B.1: Length of SMA connector and the wire used for connecting it to the antenna

Length of the SMA connector was approximately 1 cm. Length of the wire used to connect the SMA connector to the antenna was approximately

0.5 cm. Hence an extra phase coming from the 1.5 cm long electrical length which was not modeled in HFSS was then subtracted from the phase of S_{11} at all frequencies. Extra phase (θ) was calculated using the (B.1)

$$\theta(i) = \frac{2\pi\sqrt{\epsilon}_r}{\lambda(i)} \tag{B.1}$$

where,

θ= phase
$\epsilon_r = 2.2$ (permittivity of teflon)
$\lambda(i) = \frac{c}{f(i)}$

The span of frequency while taking measurements was from 600 to 1300 MHz. Hence (i) goes from 1:700. For each value of (i), there is a corresponding value of frequency starting from 600 MHz to 1300 MHz.

After calculating the extra phase at each frequency, twice of that phase was then subtracted from the measured phase of S_{11}. Twice the phase was subtracted because one for the forward going and one for the backward going EM wave. After subtracting the phase, the measured results matched closely with the simulation results.

REFERENCES

[1] E.-R. INFO, "What is RFID." [Online]. Available: www.epc-rfid.info/rfid

[2] "RFID frequency ranges." [Online]. Available: http://www.centrenational-rfid.com/rfid-frequency-ranges-article-16-gb-ruid-202.html

[3] D. M. Dobkin, *RF in RFID : Passive UHF RFID in Practice*. Burlington, MA: Newnes, 2007.

[4] "Bazooka Balun." [Online]. Available: http://www.antenna-theory.com/definitions/bazooka.php

[5] "RFID Journal." [Online]. Available: http://www.rfidjournal.com/site/faqs

[6] "Frequently asked questions." [Online]. Available: http://www.rfidjournal.com/site/faqs#Anchor-What-363

[7] "Anechoic chamber." [Online]. Available: http://en.wikipedia.org/wiki/Anechoic_chamber

[8] "3106b double ridged guide antenna." [Online]. Available: http://www.ets-lindgren.com/3106B

[9] "HFSS (high frequency structure simulator)." [Online]. Available: http://www.ansys.com/Products/Simulation+Technology/Electromagnetics/Signal+Integrity/ANSYS+HFSS

[10] "Monza 5 tag chip data sheet," Imping, USA.

[11] C. Kam, "902-928 MHz UHF RFID Tag Antenna Design, Fabrication and Test," M.S. thesis, California Polytechnic State University, San Luis Obispo, Aug. 2011.